ACS OMEGA

Open Access

http://pubs.acs.org/journal/acsodf

Review

Recent Advances in Graphene-Enabled Materials for Photovoltaic Applications: A Comprehensive Review

Pragyan Jain, R. S. Rajput, Sunil Kumar, Arti Sharma, Akshay Jain, Bhaskor Jyoti Bora, Prabhakar Sharma,* Raman Kumar,* Mohammad Shahid, Ali A. Rajhi, Majed Alsubih, Mohd Asif Shah,* and Abhijit Bhowmik

Cite This: *ACS Omega* 2024, 9, 12403−12425

Read Online

ACCESS | Metrics & More | Article Recommendations

ABSTRACT: Graphene's two-dimensional structural arrangement has sparked a revolutionary transformation in the domain of conductive transparent devices, presenting a unique opportunity in the renewable energy sector. This comprehensive Review critically evaluates the most recent advances in graphene production and its employment in solar cells, focusing on dye-sensitized, organic, and perovskite devices for bulk heterojunction (BHJ) designs. This comprehensive investigation discovered the following captivating results: graphene integration resulted in a notable 20.3% improvement in energy conversion rates in graphene-perovskite photovoltaic cells. In comparison, BHJ cells saw a laudable 10% boost. Notably, graphene's 2D internal architecture emerges as a protector for photovoltaic devices, guaranteeing long-term stability against various environmental challenges. It acts as a transportation facilitator and charge extractor to the electrodes in photovoltaic cells. Additionally, this Review investigates current research highlighting the role of graphene derivatives and their products in solar PV systems, illuminating the way forward. The study elaborates on the complexities, challenges, and promising prospects underlying the use of graphene, revealing its reflective implications for the future of solar photovoltaic applications.

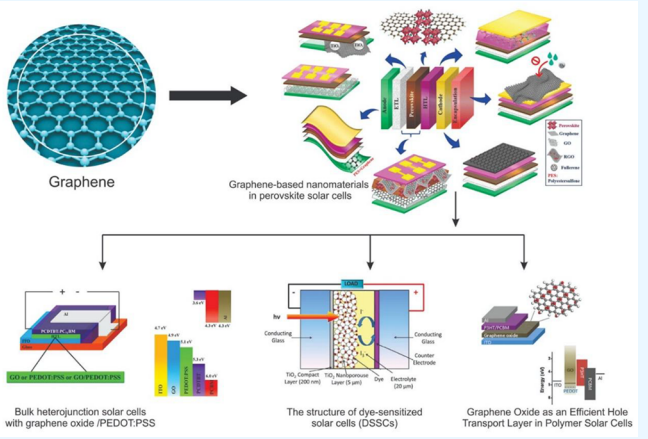

1. INTRODUCTION

Nonrenewable energy resources have a limited lifespan and cause worldwide environmental pollution. The reserve of these resources is limited, but their end products accelerate climate change and environmental degradation. Renewable energy sources are the best alternative to conventional ones as they are eco-friendly and long-term sustainable. The vast untapped energy could be harvested from solar radiation, wind, hydro, and geothermal sources. Solar energy is ample on the earth's surface and can be effectively transformed into electrical power through a suitable photovoltaic cell setup. Solar radiation is directly converted into electric energy through photovoltaic (PV) solar cells.[1] A solar PV system generally consists of several components, including a broad panel, converter, and storage devices. The conversion of solar radiation into electric energy is also influenced by the characteristics of the material employed in the device. A variety of solar cells were developed to improve efficiency. However, solar cells constantly undergo modifications and updates to enhance durability, cost-effectiveness, and solar-to-electrical power conversion efficacy.[2,3]

The energy transformation efficacy of a solar cell depends upon the materials used to develop the device.[4] It was reported that TiO_2,[5,6] ZnO, SnO_2, and organic polymers have demonstrated good optical and electronic characteristics and are found suitable as photoanode materials for dye-sensitized solar cells (DSSCs).[5,7] Silicon (Si)-based solar cells are first-generation PV cells. It is reported that the micro-crystalline silicon cell efficiency is 11.9%, while the thickness of the solar radiation interacting film is approximately 2 μm. A significant enhancement in the fill factor plays a crucial role in achieving the highest efficiency on record.[8] Second-generation solar cells are fabricated by a thin film made of thin layers of materials such as amorphous silicon, copper gallium selenide (CIGS),[9] and gallium arsenide (GaAs).[10] Advanced photovoltaic

Received: October 12, 2023
Revised: February 14, 2024
Accepted: February 23, 2024
Published: March 9, 2024

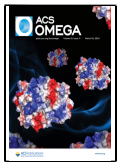

technology needs a more flexible, environmentally stable, highly photocatalytic nature and minimum electrical resistive materials. This Review comprehensively analyzed the prospect of third-generation solar cells synthesized by an ultrathin, high-conducting transparent material. Quantum-dot-sensitized solar cells (QDSSCs),[11] dye-sensitized solar cells (DSSC),[4] and perovskite solar cells[12] are viable alternatives to conventional silicon solar cells. This analysis underscores the benefits and constraints of solar cells, with a particular emphasis on the imperative to enhance power conversion efficiency (PCE). This can be achieved by integrating light conversion (LCs) phosphor materials that enable the utilization of the complete solar spectrum.[11] Graphene (GA) has recently become a showcase performer in the limelight for solar-based devices.[13]

Figure 1 depicts the carbon allotropes and successors that can be classified as 0D (fullerene), 2D (GA), and 3D (carbon nanotube).[14] GA is a successor of carbon, including carbon nanotubes, fullerenes, and carbon black.[14,15] Since armchair graphene nanoribbons are semiconducting, they are used in PV applications.[16] Notably, it has high electrical and optical properties required in various commercial applications.[17,18] GA is widely applied for the PV domain due to its high mechanical strength,[19] zero band gaps, swift carrier mobility, and desirable thermal properties.[20] Variations in molecular architecture provide different stability and characteristics to GA. Due to the meeting of the conduction band and valence band at the Dirac point (Fermi level), GA has been termed as a semimetallic semiconductor where charge carriers exhibit linear electronic dispersion.[21] The charge carriers in GA show high velocities and high mobility at 298 K. GA and its derivatives also have impressive optoelectronics, optical characteristics, and luminance properties with high thermal and mechanical strength, which varies.[22] The double bond between carbon−carbon atoms has high resistance to gas penetration and high surface area.[23] GA's internal structure, electromechanical property, and thermal response provide the main advantage for introducing its derivatives. The PCE of solar cells depends upon the transparency and thickness of the electrodes of the material. The thickness of the GA sheets varies from nano to centimeters based on the adopted synthesis process. This Review discusses the various synthesized techniques, their assistance, and restraints. This Review focuses on the research and development of graphene's potential in PV devices. Section 2 covers the synthesis methods of GA and its nanocomposites. Section 3 details the evaluation of GA for PV applications. Section 4 of this Review emphasizes the significance of genetic algorithms in perovskite solar cells. Section 5 delves into the intricacies of solar cell recycling, while section 6 concludes the study and outlines its future ramifications.

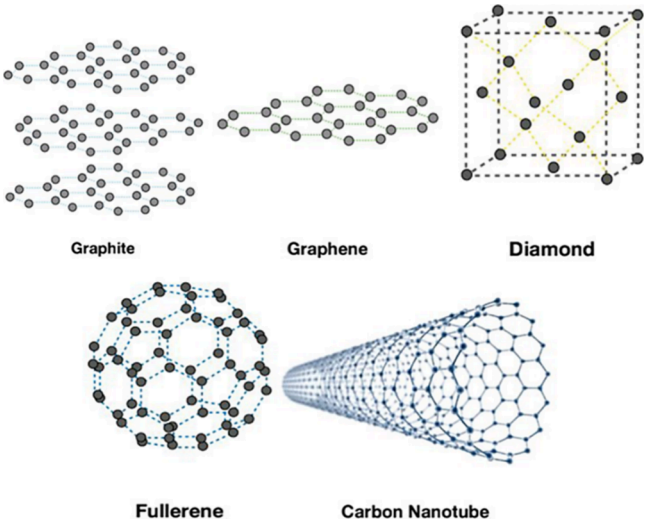

Figure 1. Allotropes of carbon and their successor.[24] Reprinted with permission from ref 24. Copyright 2010 Nature.

The structures of graphite and their derivatives, graphene oxide (GO), reduced graphene oxide (rGO), and GA, are shown in Figure 2. Graphite derivatives have been obtained, depending upon the synthesized techniques.[24,25] GO is the first derivative of graphene, also known as graphitic acid or graphitic oxide. Significant changes occur in graphite because of the functional groups in its basal plane and edges. It has various functionalities like epoxy, carboxyl, and hydroxyl.[26] These groups provide larger spacing between two consecutive layers, making interlayer spacing almost twice that of

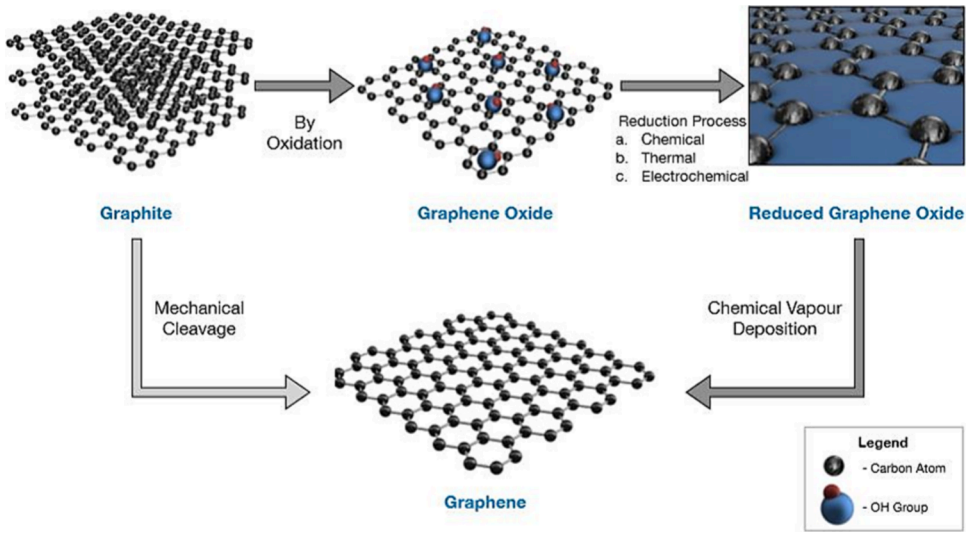

Figure 2. Preparation technique of derivatives of GA from graphite.[24] Reprinted with permission from ref 24. Copyright 2010 Nature.

https://doi.org/10.1021/acsomega.3c07994
ACS Omega 2024, 9, 12403−12425

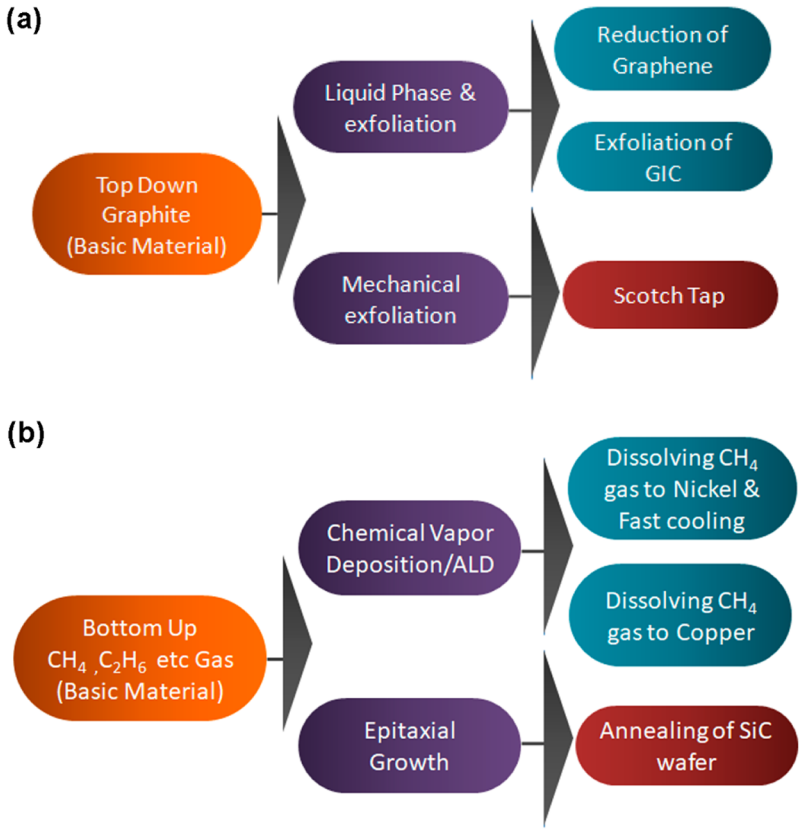

Figure 3. (a) Mechanisms of the synthesis of graphene (top-down approach).[38] (b) Mechanisms of the synthesis of graphene (bottom-up approach).[38]

graphite.[23] Several techniques eliminate these oxygen functionalities, so the surface area of rGO increases.[25] As a result, it becomes more thermally conductive, chemically reactive, and stable.[27]

Similarly, graphene quantum dots (GQDs) are related to zero-dimensional GA nanostructures and have surfaced as an emerging and promising category of materials.[28] They have lateral dimensions ranging from 2 to 20 nm, which provides better photoluminescence properties, high transparency, sensitivity, and a large surface area.[29] These properties give new hope for a remarkable and fast display system.[30] In general, GA is found in single or multilayer formations with a separation equal to the diameter of a carbon atom.

2. SELECTION OF SYNTHESIS METHOD FOR GA AND ITS NANOCOMPOSITES

The synthesis technique depends on the fundamental properties of GA, such as morphology, interlayer separation, crystal size, electron mobility, thermal behavior, solubility, and optical response. Two top-down and bottom-up approaches are primarily followed for GA synthesis.[31] The graphite turns into GO through a top-down strategy[32] by chemical oxidization or electrochemical and mechanical exfoliation. After that outcome, the product can also be reduced thermally and chemically to get the other derived rGO of graphite. In the mechanical exfoliation method, GA is produced by peeling the outer layer of graphite with a scorching tap.[33] Graphite intercalation compounds (GIC) form through mechanical energy by overcoming the van der Waals attraction force among layers. Other GA synthesis methods, that is, bottom-up, started from gas molecules as a precursor.[34] Chemical vapor deposition (CVD)[35] and atomic layer deposition (ALD)[36] are widely utilized techniques for GA synthesis. In the epitaxial growth technique, annealing a high-temperature silicon carbide (Si−C) crystal leaves a carbon-rich GA layer growing on its surface.[37] Figure 3a shows different synthesis mechanisms of GA.

GO is prepared by a chemical oxidization technique like the Hummers method.[39] Numerous functional groups containing oxygen atoms become affixed to the GO plane during oxidation. These functional groups could be replaced by thermal reduction.[32] The modified Hummers method can apply the steps mentioned above.[40] In this technique, GO is generated through a mixture of graphite, concentrated acids, and $KMnO_4$ in slow stirring under controlled temperature until the color changes from purple to brown.[41] Further, H_2O_2 was mixed in the solution. Due to the high-level oxidation of graphite, the color changes from brown to yellow.[42] GO is rinsed repeatedly with distilled water until the pH level reaches 4. During oxidization, the active oxygen group molecules relate to the GO surface by adsorption (noncovalent bond) or covalent bonds.[43] GO sheets comprise different oxygen groups, for example, epoxy, carboxyl, carboxylic acid, and hydroxyl.[44,45] These functional groups enhance the processing ability of GO for various applications.[21] Functional groups prevent atom aggregation and increase dispersion stability in multiple solvents.[46] This functionality enhances the strong reactivity and the solubility of nanomaterials in water and organic solvents by specific techniques such as chemical and thermal processing.[47] Functionality plays a critical role in attaining

https://doi.org/10.1021/acsomega.3c07994
ACS Omega 2024, 9, 12403−12425

magnificent properties and emerging applications. Much research has been done on its mechanical behavior, such as fracture and tensile strengths, Young's modulus, etc.[48] It was reported that the fracture strength of the monolayer GA sheet is 130 GPa, with a Young's modulus of 1.0 TPa, which shows the material film is defect-free.[49] It was described that the elastic modulus of the GA strip without restraint suspension is 0.25 TPa.[50] Moreover, GA dispersion in inorganic nanomaterials enhanced the mechanical stability of synthesized GA-based nanocomposites.[51,52] Although possessing biocompatibility, high optical transparency, and nontoxicity, the reduced thermal stability and compromised carrier mobility remain significant issues for GO.[53]

Following the chemical synthesis process, the oxygen functionalities present in the inner part of an aromatic area of GO can be eliminated to produce rGO.[35] rGO is derived from GO by thermal annealing or chemical reduction. 200 mL of deionized water is mixed with 100 mL of GO suspension and stirred well to achieve a nonhomogeneous dispersion. This solution is stirred at 400 rpm for 72 h to produce rGO.[54]

Following the reduction of GO, the elimination of functional groups leads to an increase in the surface area of rGO. However, this increase is accompanied by a decrease in the solubility of rGO. Enhancing the solubility of rGO necessitates chemical modification.[55] During the chemical modification process, there is an augmentation in functionality, thereby enhancing dispersion within solvents and improving solubility properties.[56] Due to chemical modification, the noncovalent functional group attached to rGO reinforces electrical properties without a change in structure.[57] Oxygenated functional groups are removed to restore π-bond networks.[58] The diverse oxygen functional sets could be detached via other techniques, thermodynamically and kinetically. The carboxyl and hydroxyl groups can be eradicated through heat treatment, whereas epoxy groups are removed utilizing the hydrazine compound.[59] The outcome of this reduction technique is called rGO; the most apparent is the derivative of GO, which shows characteristics similar to those of GO.[60] However, the π-network is redeveloped during the reduction of the material's conductivity.

Graphene is an arrangement of nanosize atoms in monolayers or multilayers. The sp^2 hybrid carbon is arranged in a honeycomb structure.[61] Most researchers established that GA is a perfect material for electrical conduction.[62] It behaves like a zero bandgap semiconductor, thus facilitating the transport of excessive electrons.[63] At room temperature, the reported value of charge mobility was 15 000 $cm^2/(V{\cdot}s)$.[62] The charge carrier mobility increases tremendously by minimizing the doping at the ambient condition observed at about 200 000 $cm^2/(V{\cdot}s)$.[64]

Furthermore, it was also described that in GA sheets, the mobility of the charge carrier is independent of the temperature.[65] The thermal conductivity of freely suspended monolayer GA was 5000 W/(m·K) using confocal micro-Raman spectroscopy.[66] This thermal characteristic is notable for electronic applications, fuel cells, and batteries because this feature of GA provides thermal stability and durability. Furthermore, GA shows a high optical conductive response. It was observed that many GA nanocomposites exhibit optical transparency.[67,68]

The chemical vapor deposition (CVD) approach is well-recognized as a prominent technology for preparing graphene-based materials. This method enables the fabrication of single- or multiple-layer structures that exhibit notable characteristics such as enhanced electrical conductivity, increased electron mobility, substantial surface and volume ratio, and notable optical response.[69] The optical characteristics of a material indicate its ability to effectively absorb solar radiation and transform the energy carried by photons into either heat or electrical energy.[70] As per the surface expanse, GA has a larger surface area than other allotropes of carbon. The large surface area of GA also provides strong interfacial interaction with other materials, atoms, or matrices during the fabrication of nanocomposites. Moreover, with the presence of minimum functionality, the large surface of GA inhibits or minimizes the cluster of particles in nanocomposites.[71,72]

GA quantum dots (GQD) are 0D particles with quantum significance and energy traps, providing photoluminescence attributes.[73] The contribution of these optical characteristics in photovoltaics means developing advanced electronics for solar cells. The prism array encapsulation structure of polymer thin film coating on solar cells improves its optical energy conversion efficiency due to size spacing variation and structure quality.[74] Graphene coatings can also be utilized for nonreflective coatings for solar cells. GQD can be synthesized by either the top-down (Table 2) or the bottom-up (Table 1) method.[75] In the top-down method, it is prepared by chemical or thermal exfoliation. This approach is favorable for fine-size production and excellent morphology. In the bottom-up technique, CVD is preferred for a homogeneous control size layer.[28]

In the bottom-up technique, the CVD process is generally used to yield pure, large-area, and high-performance GA. In this technique, the GA layer is grown on the substratum of metallic or semiconductor wafers by deposition of hydrocarbon vapor. There is a possibility that more than one gaseous vapor (precursor) decomposes on the metallic surface as per the demand of the device. The substrate surface acts as a catalyst; when the precursor flows on the stimulus, it gets deposited, and a chemical reaction occurs. The selected catalyst is either monomaterial or an alloy of more than one metal, per the requirement. The deficient d orbital metals (e.g., Co, Ni, and Cu, etc., are transition metals in metallic catalysts) promptly absorb and react with deposit carbon atoms, giving good performance. Polycrystalline GA material is generated through the absorption and concentration of carbon facilitated by metallic catalysts. The significance of polycrystallinity is the resultant thermal stability.[35] To provide hole and electron transportation, doping of GA is done with metallic atoms such as gold, platinum, and boron to create p-type GA, while copper, nitrogen, and aluminum atoms are for n-type GA.[73]

It is reported that high sustainability and nontoxicity properties are most beneficial in the case of dye-sensitized solar cells (DSSCs).[76] Recently, many researchers have testified that using GA as a quantum dot increases the power transformation competence of solar PV cells.[77] The synthesized GA properties depend upon the flow of hydrocarbon gas vapor (precursor), the pressure of a gas, the temperature, and the property of the metallic material surface.[78] Therefore, the GA structure aggregation of carbon molecules must be avoided. It was reported that the 30-in. GA layer was deposited onto the Cu wafer for roll-to-roll production by the CVD technique.[79]

Temperature is an essential factor in the CVD technique. Stefanos et al.[36] reported that between the temperature range 970−1070 °C, the activation energy enhances about 3.01 eV,

https://doi.org/10.1021/acsomega.3c07994
ACS Omega 2024, 9, 12403−12425

Table 1. A Succinct Account of the Origins and Development of Bottom-Up Graphene

technique	standard size: vertical depth	standard size: horizontal scale	advantage and limitation	ref
restricted self-organization	single-layer graphene	hundreds of nanometers	advantage: thickness control enables precise adjustments, ensuring uniformity and desired material properties limitation: even with precise thickness control, defects could impact the overall quality and performance of the material	40,81
CVD	graphene sheets with a minimal number of layers	very large scale, measured in centimeters	advantage: the product exhibits large size and high quality due to careful production limitation: the small production scale may limit overall output and availability	82−84
arc discharge	graphene including single-layer, bilayer (consisting of two layers), and few-layer forms sheets	few hundred nanometers to a few micrometers	advantage: the process can produce approximately 10 g/h of graphene, allowing for a reasonable production rate limitation: however, the low yield of graphene and the presence of carbonaceous impurities may impact the overall quality and efficiency of the production process	85
epitaxial development on silicon carbide (SiC)	few-layer graphene sheets	up to several centimeters	advantage: the production process yields an extensive area of pure graphene, providing ample material for various applications limitation: the production scale remains relatively small, limiting the quantity of graphene produced at a time	34,60,86
deconstruction of carbon nanotubes	multiple-layered nanoribbons	few micrometers long	advantage: the size control achieved by selecting starting nanotubes allows for tailored and specific graphene dimensions, catering to diverse application needs limitation: however, the process involves using expensive starting materials, which can increase production costs; the resulting graphene may also contain oxidized impurities that could affect its properties and performance in certain applications	87
reducing the oxidation of carbon monoxide (CO)	formation of multiple-layered graphene sheets	submicrometer range	advantage: the graphene sheet remains unoxidized, preserving its unique properties and ensuring high conductivity and strength limitation: however, a notable limitation is the contamination of the graphene sheet with a-Al_2O_3 and a-Al_2S, which can adversely impact its performance in certain applications and require additional purification steps	88

Table 2. A Brief Account of the Evolutionary Path of Top-Down Graphene

technique	standard size: vertical depth	standard size: horizontal scale	advantage and limitation	ref
nanolayer delamination	multilayer graphene	dimensions ranging from micrometers (μm) to centimeters (cm)	advantage: the production process yields large-sized and unmodified graphene sheets, ensuring high quality and versatility for various applications limitation: however, the production scale remains very small, which limits the overall quantity of graphene sheets that can be produced at a time	33
graphite ultrasonication	formation of both single-layer and multiple-layer graphene	in range of micrometers (μm) or even smaller, submicrometer (subμm) sizes	advantage: the graphene produced is unmodified and cost-effective, making it accessible for various applications without additional processing costs limitation: however, the production process suffers from a low yield of graphene, and the separation of the material may be challenging, impacting overall efficiency and scalability	89
electrochemical delamination/modification of graphene	monolayer and low or multilayer graphene	typically in the range of 500−700 nm	advantage: the single-step functionalization and exfoliation process results in highly conductive graphene with improved properties for various applications limitation: however, the cost of ionic liquids used in the functionalization process can be a significant factor, potentially increasing the overall production cost of the functionalized graphene	90
graphite superacid dissolution	primarily yields single-layer graphene	ranging from 300 to 900 nm	advantage: the production of unmodified graphene is scalable, allowing for large-scale manufacturing to meet market demands limitation: however, the process entails the use of hazardous chloro-sulfonic acid, which poses safety and environmental concerns; moreover, the cost and complexity of acid removal during the production process can impact the overall economic feasibility and sustainability of the process	91

https://doi.org/10.1021/acsomega.3c07994
ACS Omega 2024, 9, 12403−12425

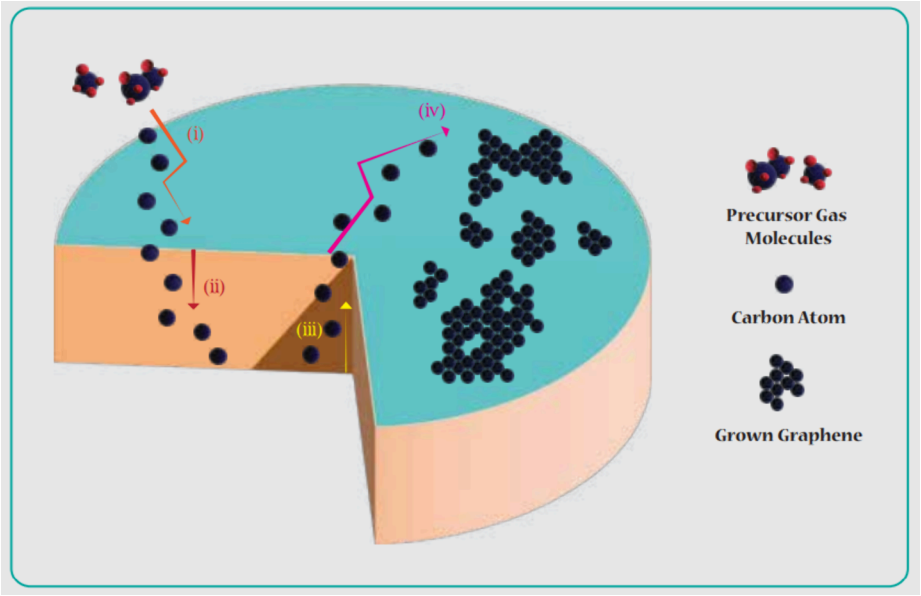

Figure 4. GA thin sheet grown on a metallic surface by the CVD technique.[73] Part (i) shows the precursor, part (ii) represents the absorption of carbon atoms, part (iii) denotes segregation, and part (iv) denotes the catalytic process.

and the growth rate increases. No extra nucleation above or below the initial layer has been detected in the uniformly grown single layer on the substrate. A highly pure and flawless GA layer typically grows under low-pressure conditions. The nucleation density is obtained from 5 to 80 nuclei/10 000 μm^2. The growth rate of the GA lies between 150 and 1400 μm^2 per 20 min.[36]

Arif et al.[80] reported negligible water intercalation within graphene oxide layers; the relative humidity is very low, about ~30%. The water adsorption on the surface and wettability are as low as the thickness of graphene layers. In the single layer (which had a thickness of 1.3 nm), the relative humidity was observed at 10%, while in the double-layer graphene (which had a thickness of 2.6 nm), the relative humidity was 80%. This improvement occurs because of the embolism of H_2O between GA layers. It was also observed that in the range of low humidity regime (5−50%), the friction force occurs from 5.9 to 8.2 nN, while the regime range increases up to 50−80%, and the friction force simultaneously rises from 8.9 to 16.5 nN.[36] Figure 4 shows that the GA thin sheet grows on a metallic surface by the CVD technique: part (i) shows the precursor, part (ii) represents the absorption of carbon atoms, part (iii) denotes segregation, and part (iv) denotes the catalytic process.[80]

3. EVALUATION OF GA IN PHOTOVOLTAIC APPLICATION

3.1. GA in Organic Solar Cells. Organic solar cells (OSCs) are more susceptible to damage under atmospheric conditions than are their inorganic counterparts. Evaluating durability involves assessing chemical stability concerning air-induced material effects, degradation from reactions with water and oxygen, and potential deterioration of electrode materials. Previous research has highlighted degradation sources in OSCs as shown in Figure 5, including donor−acceptor phase separation, photo-oxidation of active layers and donor materials facilitated by water and oxygen diffusion, and potential interface failures, particularly between the hole transport layer (HTL) and the ITO anode.[92]

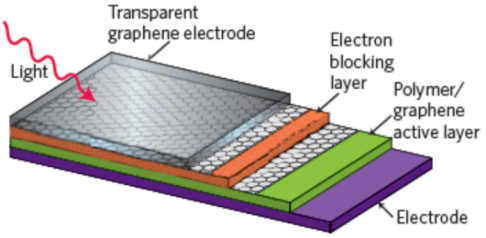

Figure 5. Schematic of organic solar cells with graphene.[97]

Addressing these challenges, the integration of carbon nanomaterials emerges as a promising solution due to their inherent barrier properties, impeding the diffusion of atmospheric elements into the device layers. Studies showcasing graphene-based materials (GRMs) in OSCs have reported enhanced long-term stability, notably in terms of preserving power conversion efficiency (PCE) over time. Recent studies have reported the long-term stability of GRM-based OSCs in terms of PCE changes.

The electrodes of an organic solar cell are a crucial element, as they are composed of materials that possess high conductivity and optical transparency. The preferred electrodes in organic solar cells are indium-doped tin oxide (ITO) and fluorine-doped tin oxide. Park et al.[93] reported that market-available ITO offers 80% transmittance in industrial applications. At the same time, on glass coating, the resistivity is about 10−15 Ω/□. Fluorine-doped tin oxide is also a candidate similar to ITO for electrodes. However, the major challenge with ITO is its cost as it is a rare earth metal, it is sensitive to higher and lower pH values, and it has brittleness, manufacturing issues, etc.[94] The solar cell industry requires flexible (avoiding brittle ITO layers), durable, conductive, thermally stable materials with high optical transparency to substitute ITO. Thus, metal grids, organic compounds, carbon nanotubes, and metal oxides are used as electrode ITO alternatives. However, due to poor optical transparency, such materials are not viable candidates for the electrode of organic PV cells.[93,94] However, due to the great properties of GA, it

https://doi.org/10.1021/acsomega.3c07994
ACS Omega 2024, 9, 12403−12425

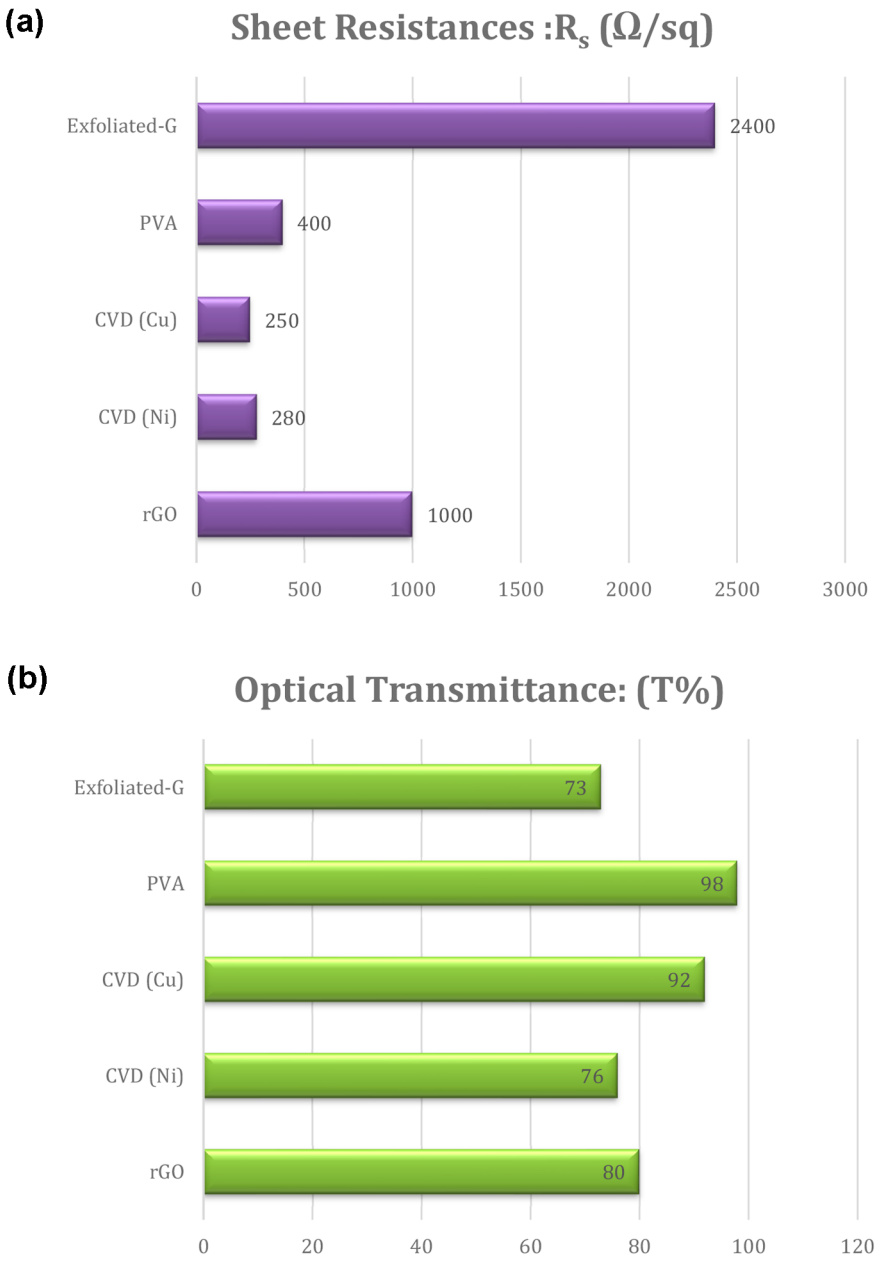

Figure 6. (a) Sheet resistance (R_s) (*PVA-poly(vinyl alcohol)). (b) Optical transmittance (T) of GA gained from diverse methods. (The purity of Ni and Cu in CVD is approximately 99.99%, and so they are utilized as the thin foil on solar cells.)

can be preferred for the electrodes of organic solar cells (OSCs).[95,96]

The comparative performance study of different materials used for OSC electrodes with and without GA shows that GA-based electrode performance easily exceeds that of ITO.[98] GA is a far better material for both anode and cathode than ITO. Graphene-based electrodes are discovered to enhance the solar conversion efficiency of OSCs.[99] GA can be utilized for a cost-effective fabrication process for OSCs at a large scale, making GA a suitable candidate for substituting ITO.[100,101] It is observed that the GA properties depend on the synthesis mechanism. CVD is a widely applied synthesis mechanism of GA to achieve a dynamic optical nature. The transmittance (T) is a significant parameter of photovoltaic systems. The value of T decreases with the increases in the width of the GA sheet, its conductivity, and the purity of materials. However, the transmittance of GA samples synthesized by CVD is poor as compared to the Hummers method, but the purity of GA is higher in CVD.[82,83] GA synthesized by CVD has better transparency and conductance properties than those synthesized by the Hummers method. GA manufactured through the Hummers technique comprises sp^3-carbons and structural defects.[102] This confines the π-bond linkages and reduces its charge carrier mobility. Also, CVD generates bigger GA sheets (<30 in.) with large conductivity and governable sheet numbers, which results in solar device performance.[84] These properties of synthesized GA play an excellent role in organic solar devices.[103] It is reported that OSCs are generally fabricated through CVD.[104] At the top layer, CVD-synthesized GA is used due to its higher transparency. Solar cells having a

https://doi.org/10.1021/acsomega.3c07994
ACS Omega 2024, 9, 12403−12425

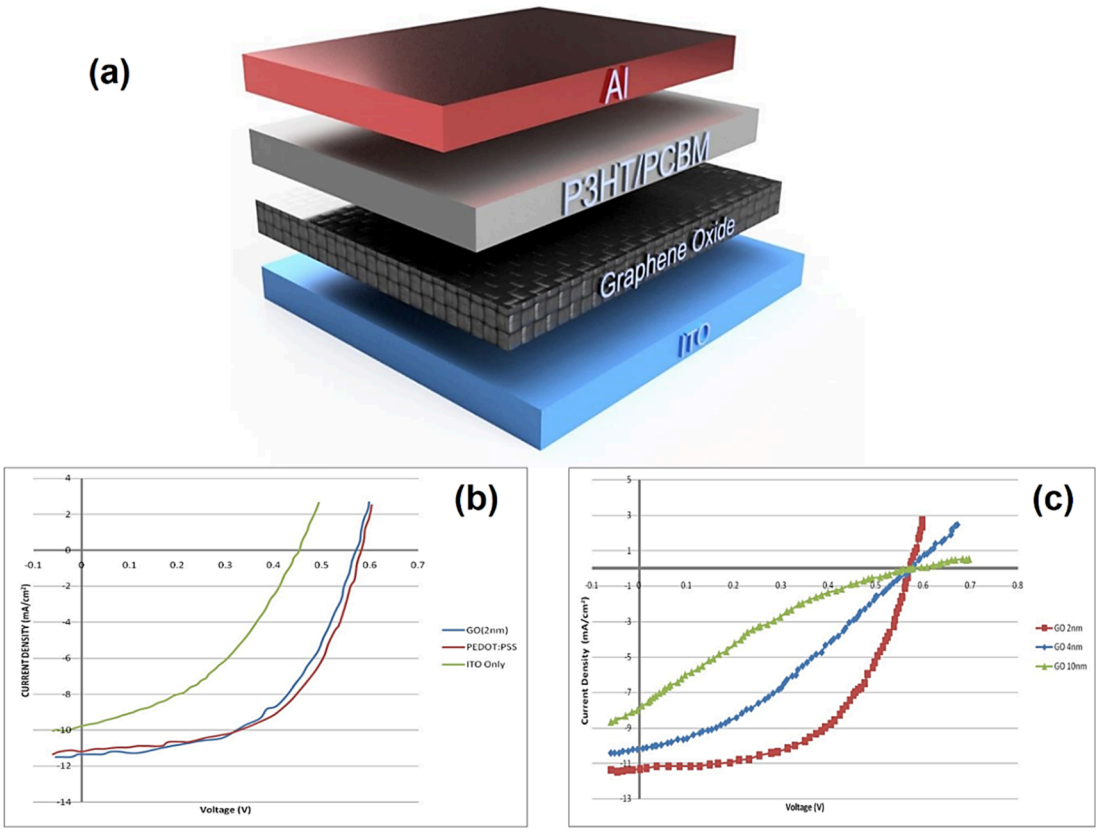

Figure 7. (a) ITO/GO/P3HT depiction: PCBM/Al photovoltaic device. (b) Behavior of PV devices without a hole transport layer as $I-V$ curves. (c) $I-V$ characteristics of the ITO/GO/P3HT:PCBM/Al devices with GO thickness variation.[120]

four-layered GA structure, good air sustainability, and high flexibility provide the efficiency of photo energy conversion up to 3.2% with 90% transmittance of GA-based electrodes. This multilayered transparent CVD synthesized by a GA-based electrode provides a long-life work capability.[96]

Li et al.[52] reported that multilayer GA is superior due to its conductivity, low transmittance, and good stability in air. The liquid exfoliation is preferred to synthesize the monolayer, bilayer, and trilayer GA, respectively. The single-, bi-, and trilayer GA synthesized by liquid exfoliation offers resistances of ∼150, 20, and 8 kΩ and transparencies of 93%, 88%, and 83%, respectively.[52] Thus, the best equilibrium among transmittance (T), resistivity (R_s), and conductivity (σ) are essential for a transparent conductive electrode. This obtained value showed that transparency decreases with an increment of R_s (Figure 6a).[52] The R_s and T values are associated with 2D conductivity (σ_{2D}) and optical conductivity (σ_o). However, conductivity depends on the synthesis technique of GA. The transmittance can be formulated as given below:[84]

$$T = [1 + (I_o/2R_s)(\sigma_o/\sigma_{2D})]^{-2} \quad (1)$$

where I_o represents the free space impedance, σ_o is optical 2D conductivity, σ_{2D} is direct current (DC) conductivity, and R_s is the electrode sheet resistance proportional to its transparency.[105] It is reported that the resistance of the electrodes depends upon the number of layers.[106] However, substrate-induced chemical doping will convert semimetallic GA to metallic GA, improving the DC conduction sufficiently to produce suitable GA realistically.[107]

The optical transmittance (T) of GA film is the crucial parameter for its performance, which is a reciprocal to conductivity and thickness, as shown in Figure 6b. The GO-based electrodes show higher T than CVD GA due to their morphological defects that help in the T of light. GA shows more than 90% T with a sheet resistance of 100−400 (Ω/□). Still, its major drawback is a low sensitivity to defects and impurities.[103] Metal nanoparticles have T = 88% with a sheet resistance R_s = 1−150 Ω/□, along with the constraints of high temperatures for sintering.[108] In comparison, carbon nanotubes show a transmittance of 82−88% and sheet resistance (R_s) = 300 Ω/□, along with an increase in resistance values at the junction of the tubes.[101,109,110]

3.2. GA as a Carrier Receiver for PV Cell. Inorganic materials utilized in solar cells possess the characteristic of efficiently absorbing solar radiation, augmenting their capacity to convert solar energy into electrical potential. The energy conversion process relies heavily on the intrinsic structure of band connections within materials. The donor and acceptor materials should possess a band alignment configuration that must be aligned in the molecular orbital that is least occupied (LUMO).[111] In acceptor and donor materials, the potential must be about 0.3 eV. To achieve good solar energy absorption, the donor element's band gap should not be higher than 1.5 eV.[112] The 2D structure is consistently supported as a receiver. Its fast charge transfer property is more compatible and suitable for donor candidates. This property shows coordination of the energy band gap.[113,114]

GA is an essential building block element in which carbon may be present in the form of several allotropes. Fullerene is one of the examples of carbon allotrope molecules. The fast charge receiving property distinguishes it from the rest of the materials. With the help of this property, organic solar cells

https://doi.org/10.1021/acsomega.3c07994
ACS Omega 2024, 9, 12403−12425

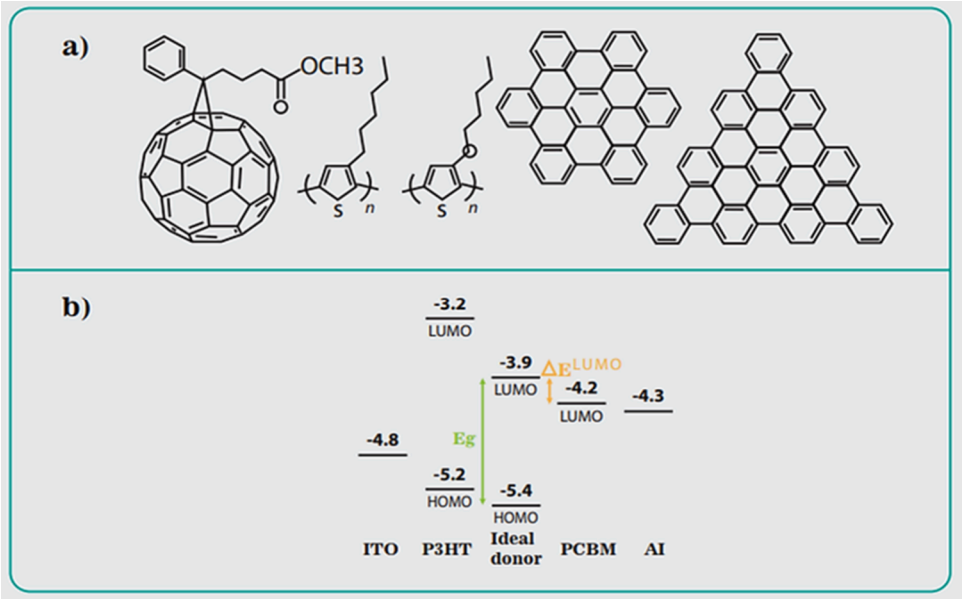

Figure 8. (a) The molecules depicted from left to right are PCBM, P3HT, P3OPT, Circ-HBC, and Tria-HBC. (b) The energy difference between acceptor and donor LUMO.

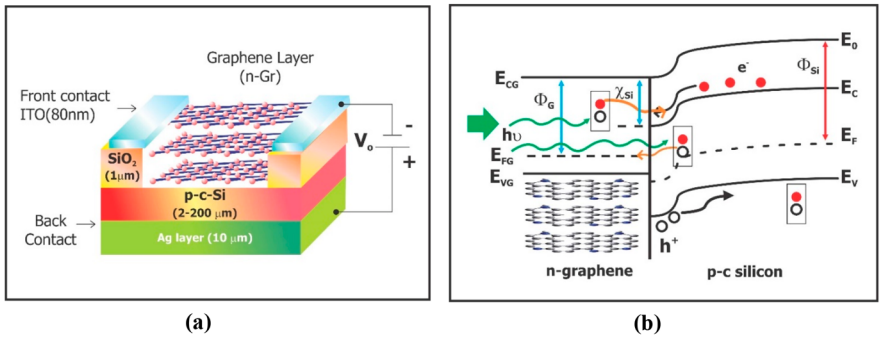

Figure 9. Graphene-based ITO photovoltaic cells and their energy band diagram.[121]

(OSCs) could be modified. Chu et al.[115] observed that the phenyl-C_{61}-butyric-acid methyl-ester (PCBM) was implemented for changing OSCs. In such ways, the GA application reveals a superior combination with donner candidates due to their inherent physical and chemical attributes.[116] The combination of the P3DT [poly(3-dodecylthiophene)]:GA depicted astonishingly less PL emissions in the about 800 nm range. Also, between 400 and 700 nm, material absorbance has been high as compared to P3OPT [poly(3-octylthiophene)].[113,114] P3HT (poly(3-hexylthiophene)) combined with GA performed a remarkable photovoltaic effect.[117] It was reported that the electrons and holes were transmitted through the material structure; selecting those materials with the highest occupied molecular orbital (HOMO) or LUMO levels[118] is necessary for a flawless transition. The thin film of GO exhibits electron blockers and good hole transfer in organic PV cells. Feng et al.[119] synthesized a PV device employing a photoactive P3HT:PCBM layer between the GO layer by synthesis of neural solution. The first layer is synthesized by indium tin oxide (ITO), which is highly conductive and see-through to provide fast radiation transmission and reduce the leakage current and recombination of electrons with holes,[112] as depicted in Figure 7. The results of the GO layer arrangement as a hole transport layer are an improvement of the PV performance proficiency as compared to the conventional hole transport layer photovoltaic device, using synthesis with PEDOT ($C_2H_4O_2C_4H_2S$) and PEDOT:PSS as the hole transportation sheet or film.[118] Figure 7b depicts that the maximum power rectangle of ITO is less than that of GO incorporation. GO incorporation eliminates the rapid erosion of ITO electrodes in PEDOT:PSS; the cause of deterioration is the acid nature of PEDOT:PSS. Figure 7c represents the open and short circuit characteristics curve; the thin film of GO improves the power conservation efficiency. This means that if the thickness is reduced, the peak power rectangle graph of the PV cell is enhanced along with the thinnest film of GO with enhanced FF and J_{sc}. Figure 7 depicts the energy band diagram of ITO PVCs.

Figure 8a shows that the molecules depicted from L to R are PCBM, P3HT, P3OPT, Circ-HBC, and Tria-HBC. Figure 8b illustrates the energy disparity between the donor and acceptor LUMO.[113,114] The LUMO donor and acceptor should have an energy difference of 0.3 eV for efficient electron transfer. The bandgap energy of the donor LUMO should be near 1.5 and 1.9 eV for P3PH.[113]

The fundamental configuration of the heterojunction solar cell consisting of graphene and silicon adheres to a TCO (ITO)/n-Gr/p-cSi/Ag arrangement, as depicted in Figure 9a.

https://doi.org/10.1021/acsomega.3c07994
ACS Omega 2024, 9, 12403−12425

Significantly, the device comprises a silicon dioxide (SiO_2) layer that functions as an insulator for carrier transport from the transparent conductive oxide (TCO) contact to the p-type crystalline silicon (p-cSi) wafer. This arrangement guarantees that transportation exclusively takes place through the graphene layer.

The solar cell with a graphene/silicon heterojunction is studied in this work. The simulation provides an illustrative depiction of the device setup (Figure 9a). Additionally, the forward-biased junction's band diagram is depicted, where Φ_G, Φ_{Si}, and χ_{Si} represent the work functions of graphene and silicon and the silicon electron affinity, respectively (Figure 9b).

3.3. GA for DSSC. Dye-sensitized solar cells, a part of the third generation of solar cell technology, are characterized by their use of thin films. The primary function of the electrode in these photovoltaic cells is to extract and collect the charge carriers. Unlike conventional solar cells, DSSCs operate differently. In these cells, photo carriers are created by dye. Initially, DSSCs were constructed using large-surface FTO plates. The thin TiO_2 film is coated on the FTO plate. This plate is a molecular sensitizer, and it is dipped into photosensitizer with another electrode like platinum. The FTO plate acts as an anode.[5] The electrodes are interconnected within the DSSCs setup, where FTO is the counter electrode. It is essential for the work function of the synthesized electron extraction material film to be low. This characteristic facilitates the easy transfer of electrons, ensuring efficient functioning within the solar cell system. It was reported that GA was used in all parts of DSSCs (Figure 10a); with the use of GA, the photo carriers drifted fast toward lithium fluoride,[114] and conjugated polymer electrolytes,[118] TiO_2, TiO_x film as n-type semiconductor, GA as an electrode for DSSCs,[122,123] and n-type organic semiconductors[115] are used as the electron transference film included in the PV cell.

It is also reported that GA as an electrode for DSSCs using ZnO improves the performance of PV devices by 36%.[125] The synthesis of GA with a width of 1 nm may be straightforwardly introduced as a channel of electron transportation in the center of the BHJ device phase.[126] PCE of these PV cells is enhanced up to 6.72% with FF = 64% and a revised value in J_{sc} = 13 mA/cm^2. In comparison, in the photovoltaic device fabricated without a GA electron transport layer (Figure 10b), the PCE is 5.35%, FF = 58%, and J_{sc} = 10.66 mA/cm^2. Figure 11a depicts the maximum power gain of the various solar cells of different material combinations. It is also reported that using GA-based ETL, the stability improved; in terms of PCE decrement with GA-based ETL, it is about 3%, while without GA-ETL, the decrement percentage of PCE is about 56% obtained in the same manner as TiO_x or GA-coated substrate, and along with GO/TiO_x, the electron transport deposit exhibits the maximum 7.5% PCE value as shown in Figure 11b.

The probes of thin-film PV cells can be developed employing material consisting of fluorine-doped tin oxide (FTO) for organic photovoltaics, DSSCs, and hybrid perovskites. Usually, the implementation of silicon PV cells becomes costly on an industrial scale.[127] Dye-sensitized cells are a rational replacement for silicon solar cells. Also, DSSC exhibited better results than conventional semiconductors. The research findings indicate that the efficiency of conversion of DSSCs exhibits improvement when the percentage of graphene oxide (GO) reduction increases.[128] This improvement can be attributed to GO's improved conductivity and

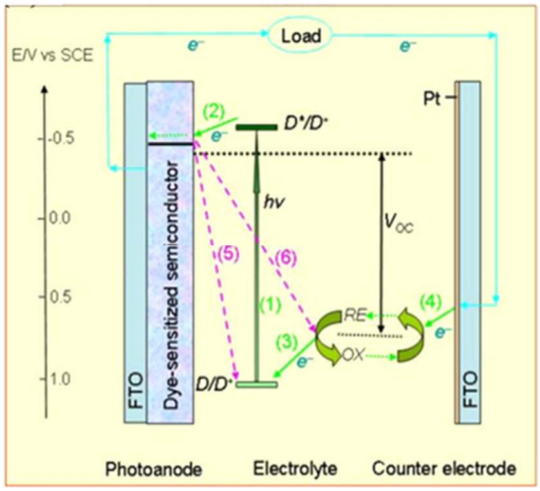

(a)

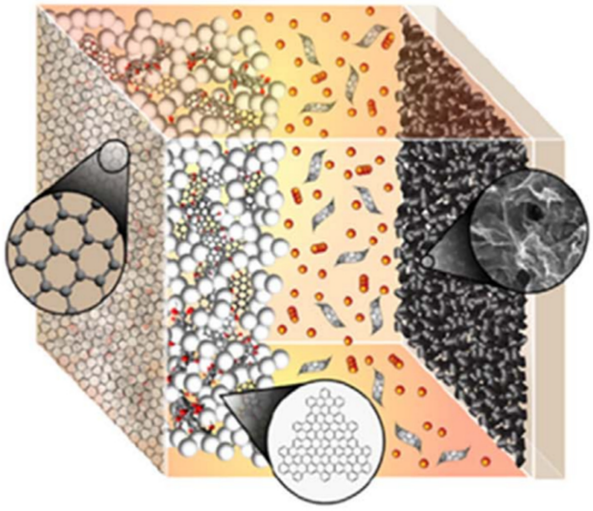

(b)

Figure 10. (a) Dye-sensitized solar cells (DSSCs)[4] and (b) incorporation of GA in all parts of DSSCs.[124]

charge mobility, following the elimination of oxygen during the reduction process.[129] The energy generation principle of DSSC is based on the photoelectric production of an electron using dye. For synthesized DSSC, a skinny transparent layer of fluorine-doped tin oxide (FTO) coated on titanium dioxide (TiO_2) comprises a translucent anode.[130,131] This combination provides a large porous surface that performs well after the emergence of molecular sensitizer solution or photosensitive dye solution with the platinum material plate on which iodide electrolyte spreads and both are combined.[76] Usually, the solution vessel is closed off to ensure that electrolytes do not leak.

The operating concept of DSSC differs from that of normal solar cells. It is based on the photoelectric production of an electron by dye-like photosynthesis.[78] Photoexcitation of the sensitizer dye causes electron transfer inside the TiO_2 nanoparticles.[132] Following charge transfer, the dye's ground state is excited by gaining electrons from the electrolyte reductant, which is then replenished by electrolyte oxidant reduction at the counter-electrode.[132] To obtain extraordinary performance, GA could be used in each dye part. The oxygen

https://doi.org/10.1021/acsomega.3c07994
ACS Omega 2024, 9, 12403−12425

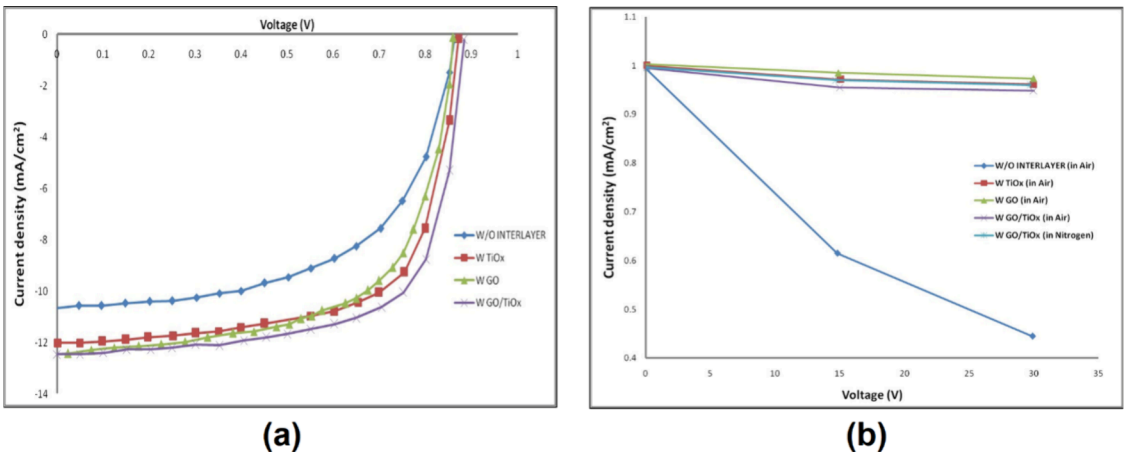

Figure 11. (a) Current density−voltage characteristics of BHJ without an ETL sheet and with ETL sheets of TiO_x, GO, and GO/TiO_x; and (b) PCE versus voltage with a GA probe in DSSCs.[126]

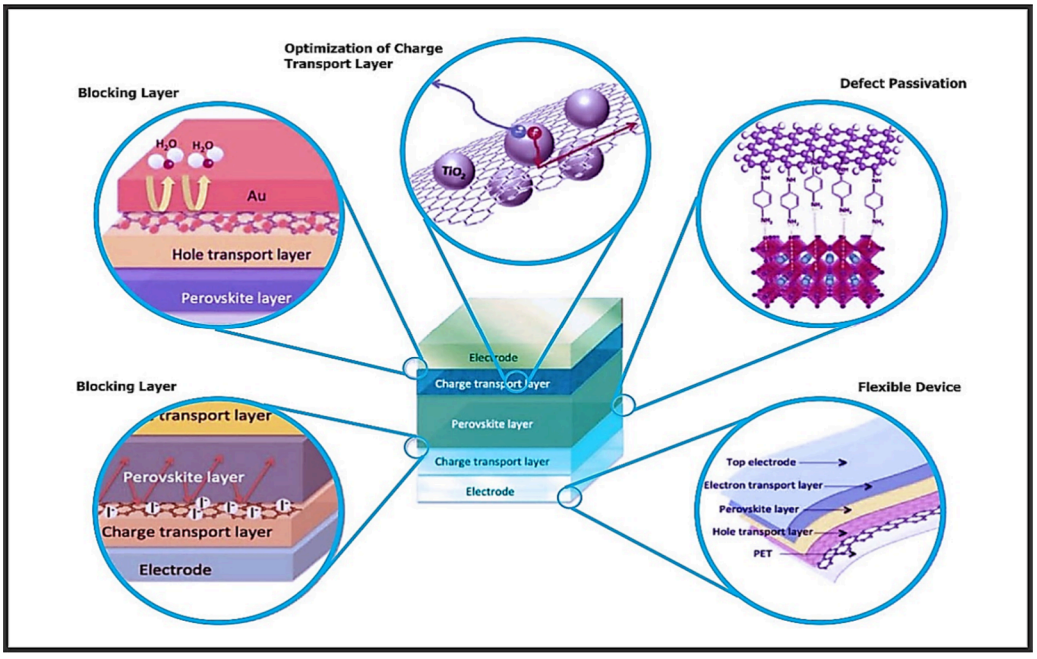

Figure 12. Schematic diagram of graphene incorporated in PSCs. Abbreviations listed: poly-ethylene terephthalate (PET), titanium dioxide (TiO_2), and gold (Au).[137]

functional group's accomplishment is vigorous in catalytic reactions. Electrolyte GA's redox chemical effect is more favorable than platinum electrodes. As compared to pure GA, doped GA performed better as counter electrodes. The scaffold shape of 3D and A is also suitable for counter electrodes.[78] In dye solar cells, PCE is enhanced by using rGO because of its high charge mobility.[132]

4. GA FOR PEROVSKITE SOLAR CELLS

Recently, halide perovskites proposed a possible material as cost-effective and more efficient for use in PV cells.[132] The first-time perovskite organo-lade halide ($CH_3NH_3PbX_3$) (X = bromine (Br) and iodine (I)) materials were used in DSSCs. With the application of inorganic materials such as Br and I, the power conversion efficiency was enhanced by 3.1% with Br and 3.8% with I, respectively.[132,133] Due to specific changes in material selection and the synthesis technique of the perovskite film, the recombination of electrons is reduced, which enhances its PCE value by an average of 16.6%.[134] Wang et al.[135] reported that in the analysis of various parameters such as lifetime, carrier diffusion length, etc., of triiodide $CH_3NH_3PbI_3$ and mixed halide $CH_3NH_3PbI_{3-x}Cl_x$ perovskite layer, the result shows that the diffusion length of $CH_3NH_3PbI_{3-x}Cl_x$ is larger than 1 μm (100 nm for $MAPBI_3$ and >1 μm for $MAPbICl_2$), there is a high carrier mobility, and there is a significant absorption coefficient that improves PCE performance of the solar cell.[136] Liang et al.[41] reported that the substrate's additive materials and film preparation technique greatly impact the perovskite surface, facilitating a high PCE of up to 12%.

The metal oxides require a high temperature for the charge transfer process. The physical structure of the PSCs is based on DSSC designs that need higher temperature fabrication owing to the usage of metal oxides that act as charge-carrying ingredients depicted in Figure 12. Different designs, such as organic photovoltaics, have addressed this issue because of

https://doi.org/10.1021/acsomega.3c07994
ACS Omega 2024, 9, 12403−12425

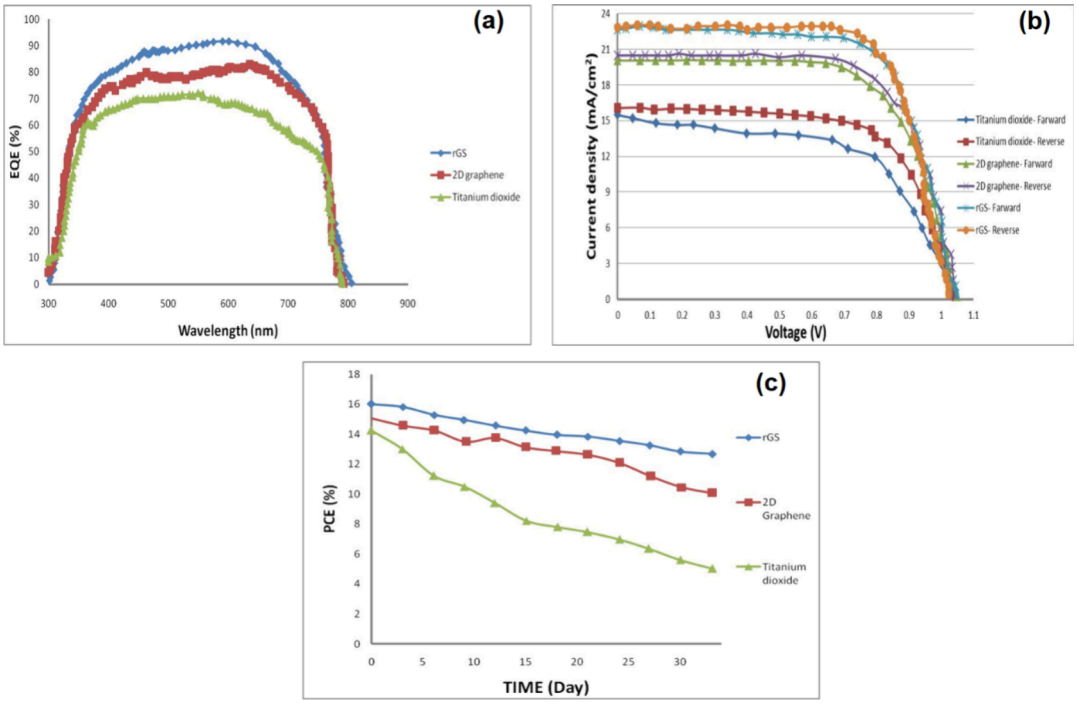

Figure 13. (a) EQE graph, (b) $J-V$ measurement, and (c) an ambient environment stability of PV cells after encapsulation through UV-cured epoxy.[145]

their easy and low-temperature manufacturing with flexible structures.[138] Liu et al.[139] described that by adopting triple material S-phenyl-C_{61}-butyric-acid methyl-ester (PCBM),[140] C_{60}, and LiF layers cathode buffer as a component in perovskites solar cell,[141] the PCE could be improved.[142] In such devices, PEDOT:PSS is arranged as an electron−hole transporter.[143] The thin LiF film promotes the carrier collection process that improves the PCE of perovskite cells by 15%.[144] Constructing a perovskite solar device using a simple composite approach with a reduced-GA scaffold (rGS) provided a large surface area.[145] This scaffold is an interfacial region among the electron transport and absorber layers in perovskite solar cells. The use of rGS was enhanced by a 17.2% PCE of PSC with a 27% overall improvement in solar cells' performance.[145] The light-trapping competence of the perovskite device and the increased superficial area in interaction with the perovskite coating contribute to a rise in the device's external quantum efficiency (EQE).[146] Figure 13 shows reduced hysteresis effects and a more extended durability than those of TiO_2-based solar PV devices.

Figure 13a represents that the electrical quantum efficiency of reduced graphene oxide is comparably high for GO film and TiO_2. It may occur due to the absence of oxygen atoms. Figure 13b depicts the comparative study between TiO_2, GA, and rGS power outcomes. The area under the curve of both biasing of rGS is large as compared to TiO_2 and GA. Further, Figure 13c denotes the PCE of all three diverse types of solar cell materials; undoubtedly, the rGS shows a response as compared to others because it does not have any oxide form. It would give good performance after a long period of use.[147] Table 3 compares the performance of various PV cell configurations manufactured with graphene, its derivatives, and other materials.

PSCs have impressive performance that outperforms organic PV cells, quantum dots PV cells, and DSSCs.[148] However, certain drawbacks have also been observed in PSC devices' material stability and mechanism. The performance of these devices decreases over time because of various influencing parameters such as exposure to thermal and moisture conditions, chemical reactions at the interfaces, etc.[148] The GA-based integration with PSCs helps to improve its device stability and performance. Table 4 reviews the GA-based PSCs device accomplishment and work strength.

Ramamoorthy et al.[149] reported that GA mixed TiO_2 thin layer blocking enhanced the efficiency of the DSSC cells. The porous nature of TiO_2 helps attach more dye molecules to its surface, improving the PCE. The Ti-GA composite functioned as a blocking layer, the metallic contact between TiO_2 and FTO glass, improving the device's performance by easing the interfacial resistance. The efficiency is also dependent on the doping percentage of GA in TiO_2. It was reported that the device's efficiency was enhanced from 2.49% to 5.09% due to fabrication in the blocking layer form.[149]

Several techniques, namely, coating, atomic layer deposition, electrochemical coating, and sputtering, are followed to develop blocking layers.[150] The efficiency of DSSC depends upon back charge transfer losses at direct (for TiO_2/dye/electrolyte) and indirect (TCO/electrolyte) pathway interfaces, respectively. The thin blocking layer suppressed this back-charge transfer and enhanced the performance of DSSC.[127,151] It was also observed from the $I-V$ characteristic that the PCE of the blocking layer solar cell obtained 5.09%. That shows the 49% increment without blocking layer cells.[151]

The electron transport in TiO_2 thin films is inhibited due to charge confining, recombination, and scattering effects of grain boundary.[152,153] Adding rGO into TiO_2 films can efficiently address these issues and enhance radiation absorbance and carrier mobility with less recombination of charge carriers as compared to native TiO_2 films.[154] Photoanodes comprising Au nanoparticles (GNPs) in the TiO_2 layer unavoidably

https://doi.org/10.1021/acsomega.3c07994
ACS Omega 2024, 9, 12403−12425

Table 3. Comparison of PV Device Performance Manufactured with Graphene, Its Derivatives, and Other Materials

cell configuration	role of GA	device performance parameters				synthesis methods	ref
		J_{sc} (mA/cm^2)	V_{oc} (V)	FF (%)	PCE (%)		
FTO/graphene/titanium dioxide/perovskite/spiro-OMeOTAD/gold	ETM	21.9	1.04	73	15.6	not available	138
FTO/conductive titanium dioxide/mesoporous titanium dioxide/graphene oxide/perovskite/spiro-OMeOTAD/gold	ETM	17.06	0.937	63.5	10.15	facile electrochemical method	163
FTO/conductive titanium dioxide/mesoporous titanium dioxide/methylammonium lead iodide/reduced graphene oxide/gold	HTM	11.5	0.95	60.54	6.62	reduction method	164
FTO/conductive titanium dioxide/reduced graphene oxide: mesoporous titanium dioxide/perovskite/spiro-OMeOTAD/gold	ETM	21.98	1.11	80	19.53	adapted Hummers method	165
ITO/tin dioxide: graphene quantum dots/methylammonium lead iodide/spiro-OMeTAD/gold	ETL	23.05	1.134	77.8	20.31	the chemical-bath deposition, spin-coating method, and atomic layer deposition (ALD) processes	166
graphene/molybdenum trioxide/poly(3,4-ethylenedioxythiophene):methylammonium lead iodide/zinc-stabilized sulfonate/fullerene (C60)/bathocuproine (BCP)/aluminum (Al)/lithium fluoride (LiF)	ETL	21.2	0.96	70	14.2	chemical vapor deposition (CVD) technique and the Lewis base adduct method	167
ITO/poly (3,4-ethylenedioxythiophene) having poly (styrene sulfonate) and graphene oxide (PEDOT:PSS-GO)/methylammonium lead iodide-chloride ($CH_3NH_3PbI_{3-x}Cl_x$)/PCBM/spiro-OMeTAD/bis(4-*tert*-butylphenyl)-benzidine (sBphen)/silver (Ag)	HTL	22.06	1.03	71	16.11	adapted Hummers method	168
graphene/molybdenum trioxide mixed with PEDOT:PSS/methylammonium lead iodide ($CH_3NH_3PbI_3$)/C_{60}/bathocuproine (BCP)/lithium fluoride (LiF)/Al	ETL	21.5	1.06	75	17.1	Lewis bases adduct method	169
FTO/conductive titanium dioxide/mesoporous titanium dioxide/graphene oxide-lithium/perovskite/spiro-OMeOTAD/gold	ETM	19.61	0.859	70.3	11.8	solution-process methods	170
FTO/ITO/graphene oxide (GO)/methylammonium lead iodide-chloride ($CH_3NH_3PbI_{3-x}Cl_x$)/phenyl-C61-butyric acid methyl ester (PCBM)/zinc oxide (ZnO)/gold (Au)	HTM	17.46	1.00	71	12.4	modified Hummers method (MHM) solution-precipitation process	168
FTO/titanium dioxide/titanium dioxide-perovskite/perovskite/graphene	ETL	16.7	0.943	73	11.5	MHM	171
FTO/titanium dioxide/perovskite/spiro-OMeOTAD/poly(3,4-ethylenedioxythiophene):polystyrene sulfonate (PEDOT:PSS)/graphene	ETL	17.75	0.945	71.72	12.03	chemical vapor deposition (CVD) method layer-by-layer stacking method	172
ITO/poly(3,4-ethylenedioxythiophene):polystyrene sulfonate (PEDOT:PSS)/self-stacked solvated graphene (SSG)/methylammonium lead iodide-chloride ($CH_3NH_3PbI_{3-x}Cl_x$)/phenyl-C61-butyric acid methyl ester (PCBM)/aluminum (Al)	HTM	22.6	0.92	70.1	14.51	chemical vapor deposition (CVD), simple vacuum filtration, and the hydrothermal approach	173
graphene/molybdenum trioxide mixed with poly(3,4-ethylene dioxythiophene):polystyrene sulfonate (PEDOT:PSS)/methylammonium lead iodide($CH_3NH_3PbI_3$) /fullerene (C_{60})/bathocuproine (BCP)/lithium fluoride (LiF)/aluminum (Al)	ETL	22.5	1.03	74.3	17.3	one-step fast deposition crystallization method	174
reduced graphene oxide (rGO) coated with mesoporous titanium dioxide (mp-TiO_2), deposited on top of a blocking layer of titanium dioxide (TiO_2)/methylammonium lead iodide ($CH_3NH_3PbI_3$)/spiro-OMeTAD/lithium bis (trifluoromethane sulfonyl)imide (Li-TFSI)/*tert*-butyl pyridine (TBP)/silver (Ag)	ITEM	20.02	0.89	71.2	12.7	sequential deposition method and spin-coating method	164
doped amorphous silicon (a-Si) solar cell with an interdigitated back contact (IBC) structure, utilizing a transparent conductive oxide (TCO) layer	ETL/NIL	42.3	0.744	83.8	26.3 ± 0.5	PECVD method or hot-wire CVD method	175
PERL and PERT(either localized p+ doping (PERL) or diffused p+ doping (PERT)/inverted pyramid, passivation	NIL	42.20	706.0	82.80	24.70	sequential deposition method	176

https://doi.org/10.1021/acsomega.3c07994
ACS Omega 2024, 9, 12403−12425

Table 4. A Brief Review of the GA-Based PSCs Device Performance and Its Stability[143]

device architecture	types	device stability performance	ref
FTO/titanium dioxide (TiO_2)//methylammonium lead iodide ($MAPbI_3$) with graphene nanofibers/spiro-OMeTAD/gold (Au)	perovskite	the device's initial PCE was found to be 94% after 150 h of working and reduced to 89.5% after 300 h having 85% RH	12
ITO/graphene oxide (GO)/methylammonium lead iodide ($MAPbI_3$) with graphene oxide (GO)/phenyl-C_{61}-butyric acid methyl ester (PCBM)/silver (Ag)	perovskite	more than 2000 working hours, the power conversion efficiency (PCE) of the device was 80% of its initial PCE under 50% RH	177
FTO/block titanium dioxide/mesoporous titanium dioxide/formamidinium-methylammonium lead iodide-bromide ($FA_{0.85}MA_{0.15}Pb(I_{0.85}Br_{0.15})_3$) with nitrogen-doped reduced graphene oxide (N-rGO)/spiro-OMeTAD/gold (Au)	perovskite	not available	178
FTO/conductive titanium dioxide/mesoporous titanium dioxide/methylammonium lead iodide ($MAPbI_3$) with graphene quantum dots (GQD)/spiro-OMeTAD/gold (Au)	perovskite	not available	179
FTO/alpha-iron(III) oxide (α-Fe_2O_3)/methylammonium lead iodide ($MAPbI_3$) with nitrogen-doped surface-functionalized graphene quantum dots (NSGQDs)/hole transport layer (HTL)/gold (Au)	perovskite	humidity stability improved by 78% after 400 h, and its thermal stability improved by 84% after 300 h compared to the initial PCE condition	180
FTO/conductive titanium dioxide/mesoporous titanium dioxide with graphene/perovskite/graphene oxide/spiro-OMeTAD/gold (Au)	ETM TiO_2	under continual light exposure at the peak power point, the device retained over 88% of its initial PCE after 16 h of testing; when it was exposed to thermal stability testing at 60 °C in an oven scenario, it lost 15% of its PCE efficiency	181
FTO/conductive titanium dioxide/mesoporous titanium dioxide with graphene/graphene oxide-lithium/methylammonium lead iodide ($MAPbI_3$)/spiro-OMeTAD/gold (Au)	ETM TiO_2	not available	182
FTO/conductive titanium dioxide/mesoporous titanium dioxide with graphene/methylammonium lead iodide ($MAPbI_3$) /spiro-OMeTAD/gold	ETM TiO_2	the device performance was 93% after 1 week of working in dry conditions at 30 °C in a dark place	183
FTO/conductive titanium dioxide/mesoporous titanium dioxide with graphene/zirconium dioxide (ZrO_2)/methylammonium lead iodide ($MAPbI_3$)/carbon (C)	ETM TiO_2	not available	184
FTO/conductive titanium dioxide/reduced graphene oxide with lithium-doped mesoporous titanium dioxide/$(FAPbI_3)_{0.85}(MAPbBr_3)_{0.15}$/spiro-OMeTAD/gold (Au)	ETM TiO_2	not available	185
FTO/conductive titanium dioxide/reduced graphene oxide with titanium dioxide/$(FAPbI_3)_{0.85}(MAPbBr_3)_{0.15}$/spiro-OMeTAD/gold (Au)	ETM TiO_2	not available	186
FTO/conductive titanium dioxide/mesoporous titanium dioxide/graphene oxide-lithium/methylammonium lead iodide ($MAPbI_3$)/spiro-OMeTAD/gold (Au)	ETM TiO_2	the stability of the device is improved when exposed to white light from a light-emitting diode (100 mW cm^{-2}) at room temperature for a continuous period of 60 h	187
FTO/nickel oxide (NiO)/graphene oxide (GO)/perovskite/graphene oxide-lithium (GO-Li)/titanium oxide (TiO_x)/aluminum (Al)	ETM TiO_2	after 15 days of working, the device lost 30% of its efficiency with the ambient conditions of humidity and temperature	188
FTO/zinc oxide (ZnO) with graphene (G)/zinc oxide (ZnO)/methylammonium lead iodide ($MAPbI_3$)/spiro-OMeTAD/gold (Au)	ETM ZnO	not available	189
FTO/conductive nanographene (NG) with zinc oxide nanorod nanocrystals (ZnO NR NCs)/methylammonium lead iodide ($MAPbI_3$)/spiro-OMeTAD/silver (Ag)	ETM ZnO	not available	190
FTO/zinc oxide (ZnO)/multilayered graphene (MLG)/methylammonium formamidinium perovskite (MAFA)/spiro-OMeTAD/gold (Au)	ETM ZnO	the performance of the device was reduced by 7% of the initial PCE under continuous light within 300 working hours	190
FTO/graphene-tin dioxide (G-SnO_2)/methylammonium lead iodide ($MAPbI_3$)/spiro-OMeTAD/gold (Au)	ETM SnO_2	90% of the initial PCE value was maintained after 300 h of exposure with humidity levels of 40 ± 5% and room temperature	191
$EMMBF_4$/Ag/graphene nanosheets (GNs)/tin dioxide (SnO_2)/C_{60} self-assembled monolayer (C_{60}-SAM)/methylammonium lead iodide ($MAPbI_3$)/spiro-OMeTAD/gold (Au)	ETM SnO_2	not available	192
ITO/tin dioxide nanoparticles with niobium doping (SnO_2:NGO) /$Rb_{0.05}(FA_{0.83}MA_{0.17})_{0.95}Pb(I_{0.83}Br_{0.17})_3$-cesium iodide (CsI)/spiro-OMeTAD/gold (Au)	ETM SnO_2	the addition of NGOs did not impact the device stability under ambient conditions	193
FTO/graphene-embedded tin dioxide (G@SnO_2)/cesium formamidinium methylammonium perovskite (CsFAMA-perovskite)/spiro-OMeTAD/gold (Au)	ETM SnO_2	not available	194
PEN (polyethylene naphthalate)/ITO (indium tin oxide)/graphene-embedded tin dioxide (G5@SnO_2)/cesium formamidinium methylammonium perovskite (CsFAMA-perovskite)/spiro-OMeTAD/gold (Au)	ETM SnO_2	not available	146
ITO/poly(3,4-ethylene dioxythiophene):polystyrenesulfonate (PEDOT:PSS)/methylammonium lead iodide-Chloride ($MAPbI_{3-x}Cl_x$)/reduced graphene oxide:phenyl-C_{61}-butyric acid methyl ester (rGO:PCBM)/polyethylene naphthalate (PEN)/silver (Ag)	PCBM	50% of initial PCE was maintained after 50 working hours with prolonged solar illumination and relative humidity (>50%)	195
ITO/graphene quantum dots:phenyl-C_{61}-butyric acid methyl ester (GQD:PCBM)/methylammonium lead iodide ($MAPbI_3$)/spiro-OMeTAD/gold (Au)	PCBM	the device maintained more than 80% of the original PCE value for 300 working hours with simulated sunlight and full ultraviolet component presence	196
APTES-functionalized graphene (APTES-GR)/phenyl-C_{61}-butyric acid methyl ester:graphene quantum dots (PCBM:GQDs)/gold (Au)	PCBM	not available	197

https://doi.org/10.1021/acsomega.3c07994
ACS Omega 2024, 9, 12403−12425

Table 4. continued

device architecture	types	device stability performance	ref
ITO/titanium dioxide (TiO_2)/methylammonium lead iodide chloride ($MAPbI_3Cl_{3-x}$)/reduced graphene oxide (rGO)/spiro-OMeTAD/gold (Au)	HTM spiro-OMeTAD	the device containing rGO shows higher stability while kept under constant sunlight in a nitrogen-filled glovebox	198
ITO/tin dioxide (SnO_2)/methylammonium formamidinium perovskite (MAFA-perovskite)/reduced graphene oxide (rGO) mixed with spiro-OMeTAD/gold (Au)	HTM spiro-OMeTAD	the efficiency of 75% of its initial PCE values was maintained after 500 working hours in ambient conditions (40−60% humidity)	199
ITO/poly(3,4-ethylene dioxythiophene):polystyrenesulfonate:graphene (PEDOT:PSS:G)/methylammonium lead iodide ($MAPbI_3$)/phenyl-C_{61}-butyric acid methyl ester (PCBM)/ytterbium (Yb)/aluminum (Al)	PEDOT:PSS	enhanced stability of device at room operation conditions	200
ITO/graphene oxide (GO) mixed with poly(3,4-ethylene dioxythiophene):polystyrenesulfonate (PEDOT:PSS)/$(FAPbI_3)_{0.85}(MAPbBr_3)_{0.15}$/phenyl-$C_{61}$-butyric acid methyl ester ($PC_{61}BM$)/bathocuproine (BCP)/silver (Ag)	PEDOT:PSS	not available	201
ITO/poly(3,4-ethylene dioxythiophene):polystyrenesulfonate (PEDOT:PSS)/graphene oxide (GO)/methylammonium lead iodide ($MAPbI_3$)/phenyl-C_{61}-butyric acid methyl ester (PCBM)/silver (Ag)	PEDOT:PSS	the device performed at 83.5% of the original PCE after working for 39 days in the air	202
ITO/poly(3,4-ethylene dioxythiophene):polystyrenesulfonate (PEDOT:PSS)/strontium-functionalized reduced graphene oxide (SrGO)/methylammonium lead iodide ($MAPbI_3$)/phenyl-C_{61}-butyric acid methyl ester (PCBM)/bathocuproine (BCP)/silver (Ag)	PEDOT:PSS	the device stability is enhanced in the ambient environment as per the ISOS-D-1 protocol	203
ITO/reduced graphene oxide (rGO)/copper thiocyanate (CuSCN)/methylammonium lead iodide ($MAPbI_3$)/phenyl-C_{61}-butyric acid methyl ester (PCBM)/bathocuproine (BCP)/silver (Ag)	CuSCN	90% of the device's initial PCE efficiency was maintained in AM 1.5 sunlight exposure for about 100 working hours	204
FTO/titanium dioxide (TiO_2)/cesium formamidinium methylammonium lead iodide bromide ($CsFAMAPbI_{3-x}Br_x$)/copper thiocyanate (CuSCN)/reduced graphene oxide (rGO)/gold (Au)	CuSCN	the device maintained 95% of PCE after aging for 1000 h under full-sun light exposure at 60 °C temperature	205
FTO/titanium dioxide (TiO_2)/cesium formamidinium methylammonium lead iodide bromide ($CsFAMAPbI_{3-x}Br_x$)/copper thiocyanate (CuSCN)/graphene (G)/gold (Au)	CuSCN	the device maintained more than 94% of its actual PCE in relative humidity of 50% in dark conditions	206
ITO/graphene oxide (GO)/methylammonium lead iodide ($MAPbI_3$)/fullerene (C_{60})/bathocuproine (BPhen)/silver (Ag)	GA-based material as HTM	not available	207
ITO/amorphous graphene oxide (a-GO)/methylammonium lead iodide-chloride ($MAPbI_{3-x}Cl_x$)/phenyl-C_{61}-butyric acid methyl ester (PCBM)/bathocuproine (BCP)/silver (Ag)	GA-based material as HTM	the device retained 90% of its initial power conversion efficiency (PCE) after operating for 30 days in a dry nitrogen gas atmosphere	208
ITO/reduced graphene oxide (rGO)/methylammonium lead iodide ($MAPbI_3$)/phenyl-C_{61}-butyric acid methyl ester (PCBM)/bathocuproine (BCP)/silver (Ag)	GA-based material as HTM	the device preserved 62% of its power conversion efficiency (PCE) after 140 h of exposure to light without encapsulation under ambient conditions with around 50% humidity	209
ITO/reduced graphene oxide (rGO)/methylammonium lead iodide ($MAPbI_3$)/phenyl-C_{61}-butyric acid methyl ester (PCBM)/silver (Ag)	GA-based material as HTM	the device sustained a 50% power conversion efficiency (PCE) after 1000 h of continuous operation without encapsulation at 25 °C and 30% relative humidity	210
ITO/fluorine-functionalized reduced graphene oxide (F-rGO)/methylammonium lead iodide ($MAPbI_3$)/phenyl-C_{61}-butyric acid methyl ester ($PC_{61}BM$)/bathocuproine (BCP)/silver (Ag)	GA-based material as HTM	the power conversion efficiency (PCE) remained at 72% of its initial value for a duration of 30 working days under ambient conditions, with a humidity level of 50% and a temperature of 25 °C	211
FTO/titanium dioxide (TiO_2)/methylammonium lead iodide ($MAPbI_3$)/reduced graphene oxide (rGO)/gold (Au)	GA-based material as HTM	the device maintained 50% of its initial power conversion efficiency (PCE) value for 30 days in an open ambient atmosphere without any encapsulation	212

https://doi.org/10.1021/acsomega.3c07994
ACS Omega 2024, 9, 12403−12425

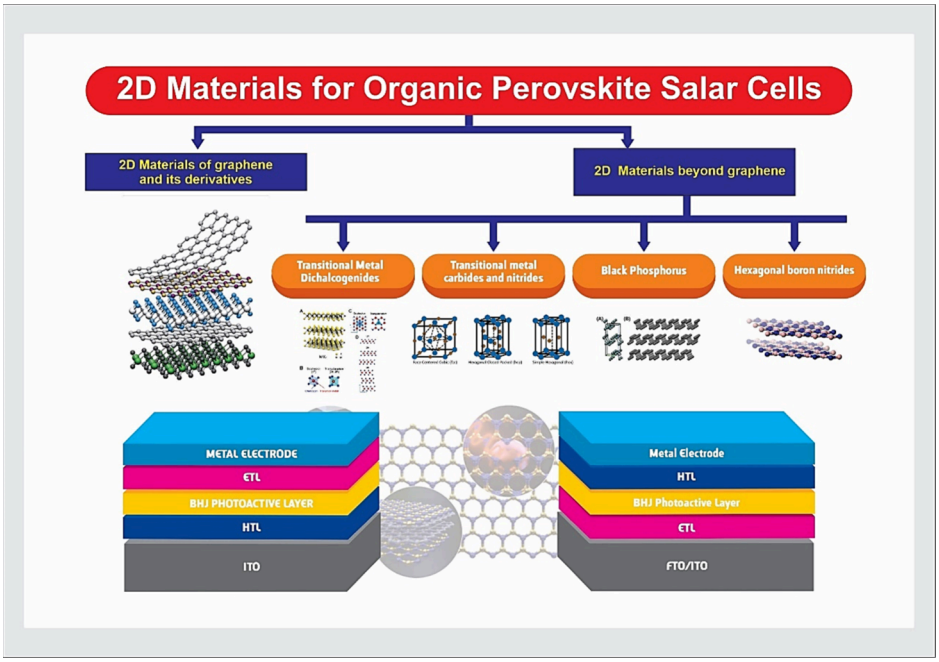

Figure 14. ITO and FTO-based electrodes in the photovoltaic device.[156]

experience oxidation at high temperatures; hence, GNPs turn into reduced GO.[155] Morphological analysis revealed that defectless thin layers were produced due to the integration of rGO. The band gap value found in the TiO_2−rGO layer was 3.34 eV, while it was 3.37 eV for TiO_2.[154]

5. GA AND OTHER MEMBERS OF 2D MATERIALS FOR ADVANCED SOLAR CELLS

GA belongs to the 2D materials family; other 2D materials have gained attainment because of their optical and electronic characteristics for the evolution of PV cells and other optoelectronic devices. Some 2D materials with zero band gap material act as semiconductors. Such semiconductors are also utilized as thin, flexible PV cells.

Figure 14 depicted 2D materials for photovoltaic applications, categorized into GA and GA derivatives, and other 2D materials, including GA, transition-metal dichalcogenides (TMDCs), black phosphorus (BP), and boron nitrides. These materials play essential roles in enhancing the performance and stability of thin-film solar cells, presenting exciting opportunities for advancements in solar energy technology.

Several reported works show that 2D materials, like TMDCs[157,158] and black phosphorus,[159] have evolved rapidly because of their exceptional mechanical characteristics, light weight, high tensile strength, and high young modulus. This helps in designing flexible and stretchy next-level electronic devices.[160] Si-based PV cells have gained popularity in renewable technology due to their high PCE and cheap electric power generation. The GA is also utilized as transparent and conductive electrodes in solar cell technology. The conductivity of GA improves with a rise in the number of layers due to poor transparency. Thus, a proper trade-off should be done to achieve the optimum performance of GA electrodes.[160]

The sheet resistance of GA is lowered through its doping process to optimize the inner potential of Si-PV cells. The ambipolar characteristic of gallium arsenide (GA) enables the incorporation of both an anode and a cathode, as well as electron transport layers (ETL) or hole transport layers (HTL), in organic and perovskite photovoltaic (PV) cells. Furthermore, there is a strong likelihood that gallium arsenide (GA) will play a crucial role as a ternary substance in organic photovoltaic (PV) cells and as a material employed for stabilization.[161] In recent years, significant research has been conducted on using 2D materials in solar cell applications, particularly on molybdenum disulfide, molybdenum diselenide, and tungsten diselenide.[162] These materials exhibit advantageous properties due to their elevated absorption coefficient within the visible and infrared regions of the solar spectrum. The optimization of the work function, as well as the bandgap of transition metal dichalcogenides (TMDCs), has been found to have potential applications in organic and perovskite photovoltaic (PV) cells.[162] The photovoltaic cells based on 2D heterostructures have superior absorption coefficients, elevated radiative efficiency, and well-defined interfaces, resulting in the highest power-to-weight ratio of the active material. The integration of roll-to-roll treated graphene oxide into current photovoltaic technologies is currently a prominent area of research.[162]

6. CONCLUSIONS AND FUTURE REMARKS

This Review comprehensively analyzes the utilization of GA and its derivatives GO, rGO, and GDs over conventional solar photovoltaic cells. GA has exceptional characteristics, including the absence of bandgaps, elevated carrier mobility, expansive surface area, optical responsiveness, and advantageous thermomechanical properties. The various synthesis techniques of GA are described with their limitations. This Review presents several significant findings and offers insights for future research. The transparency and transmittance of GA as the monolayer or multilayer depend on their preparation technique. The many techniques of GA preparation, like the Hummers method, epitaxial growth, and CVD technique, are proposed in this Review. By the adoption of an appropriate synthesis technique, the transparency of the GA layer can be

https://doi.org/10.1021/acsomega.3c07994
ACS Omega 2024, 9, 12403−12425

increased, which would improve the PCE of the solar cell. GA offers a 2D arrangement of carbon atoms, a large surface area with transparency capable of encapsulating solar cells.

Regardless of remarkable progress in GA-based solar cells, the mass production of graphene is still more challenging. The introduction of thin homogeneous GA layers on the substrate is another issue. Currently, many researchers are working on GA and other 2D materials to develop new synthesis methodologies of GA derivates and novel fabrication techniques of PV cells to achieve cost-effective, flexible, foil-type thin advanced PV cells that would be easy to install and are also ecofriendly.

AUTHOR INFORMATION

Corresponding Authors

Mohd Asif Shah − *Department of Economics, Kebri Dehar University, Kebri Dehar 250, Ethiopia; Centre of Research Impact and Outcome, Chitkara University Institute of Engineering and Technology, Chitkara University, Rajpura, Punjab 140401, India; Division of Research and Development, Lovely Professional University, Phagwara, Punjab 144001, India*; Email: drmohdasifshah@kdu.edu.et

Raman Kumar − *Department of Mechanical and Production Engineering, Guru Nanak Dev Engineering College, Ludhiana, Punjab 141006, India;* orcid.org/0000-0003-2934-7609; Email: sehgal91@yahoo.co.in

Prabhakar Sharma − *Department of Mechanical Engineering, Delhi Skill and Entrepreneurship University, Delhi 110089, India;* orcid.org/0000-0002-7585-6693; Email: psharmahal@gmail.com

Authors

Pragyan Jain − *Deptartment of Mechanical Engineering, University Institute of Technology, Rajiv Gandhi Proudyogiki Vishwavidyalaya, Bhopal, Madhya Pradesh 462033, India*

R. S. Rajput − *Department of Mechanical Engineering, Rajiv Gandhi Proudyogiki Vishwavidyalaya, Bhopal, Madhya Pradesh 462033, India*

Sunil Kumar − *Department of Mechanical Engineering, Rajiv Gandhi Proudyogiki Vishwavidyalaya, Bhopal, Madhya Pradesh 462033, India*

Arti Sharma − *Department of Physics and Electronics, Rani Durgavati Vishwavidyalaya, Jabalpur, Madhya Pradesh 482001, India*

Akshay Jain − *Energy Institute Bengaluru, A Centre of Rajiv Gandhi Institute of Petroleum Technology, Bengaluru, Karnataka 562157, India*

Bhaskor Jyoti Bora − *Energy Institute Bengaluru, A Centre of Rajiv Gandhi Institute of Petroleum Technology, Bengaluru, Karnataka 562157, India*

Mohammad Shahid − *Department of Electrical Engineering, Galgotias College of Engineering and Technology, Greater Noida, Uttar Pradesh 201306, India*

Ali A. Rajhi − *Department of Mechanical Engineering, College of Engineering, King Khalid University, Abha 61421, Saudi Arabia*

Majed Alsubih − *Civil Engineering Department, College of Engineering, King Khalid University, Abha 61421, Saudi Arabia;* orcid.org/0000-0001-8226-1682

Abhijit Bhowmik − *Mechanical Engineering Department, Dream Institute of Technology, Kolkata 700104, India; Chitkara Centre for Research and Development, Chitkara University, Himachal Pradesh 174103, India*

Complete contact information is available at: https://pubs.acs.org/10.1021/acsomega.3c07994

Notes

The authors declare no competing financial interest.

ACKNOWLEDGMENTS

We extend our appreciation to the Deanship of Scientific Research at King Khalid University for funding this work through a large group research project under grant no. RGP2/343/44.

NOMENCLATURE

T = transmittance
R_s = sheet resistance
2D = two-dimensional
0D = zero-dimensional
PV = photovoltaic
DC = direct current
BHJ = bulk heterojunction
GA = graphene
GO = graphene oxide
CVD = chemical vapor deposition
DSSCs = dye-sensitized solar cells
LUMO = lowest unoccupied molecular orbitals
HOMO = highest occupied molecular orbitals
PCBM = phenyl-C_{61}-butyric acid methyl-ester
PEDOT:PSS = poly(3,4-ethylene-dioxy-thiophene):poly-styrenesulfonate
P3HT = regioregular poly(3-hexylthiophene-2,5-diyl)
ITO = indium tin oxide
FTO = fluorine-doped tin oxide
TCO = transparent conductive oxide
OSCs = organic solar cells
PCE = power conversion efficiency
TiO_2 = titanium dioxide
ZnO = zinc oxide
SnO_2 = tin(IV) oxide/stannic oxide
rGS = reduced-GA scaffold
EQE = external quantum efficiency
rGO = reduced graphene oxide
ALD = atomic layer deposition
QDSCs = quantum dot solar cells
GPa = gega pascal
TPa = tera pascal
OPVs = organic photovoltaics
ETM = electronic transfer material
HTM = hole transfer material
Elect = electrode
ETL = electron transport layer
HTL = hole transport layer
PVA = poly(vinyl alcohol)
Si = silicon
TMDCs = transition-metal dichalcogenides
GNPs = photoanodes comprising Au nanoparticles
Au = gold
Cu = copper
Ni = nickel
GIC = graphite intercalation compounds
LiF = lithium fluoride
TiO_x = titanium oxide

https://doi.org/10.1021/acsomega.3c07994
ACS Omega 2024, 9, 12403−12425

REFERENCES

(1) Deka, M. J.; Kalita, P.; Das, D.; Kamble, A. D.; Jyoti Bora, B.; Sharma, P.; et al. An approach towards building robust neural networks models using multilayer perceptron through experimentation on different photovoltaic thermal systems. *Energy Convers Manag* **2023**, *292*, 117395.

(2) Gopi, A.; Sharma, P.; Sudhakar, K.; Ngui, W. K.; Kirpichnikova, I.; Cuce, E. Weather Impact on Solar Farm Performance: A Comparative Analysis of Machine Learning Techniques. *Sustainability* **2023**, *15*, 439.

(3) Le, T. H.; Pham, M. T.; Hadiyanto, H.; Pham, V. V.; Hoang, A. T. Influence of various basin types on performance of passive solar still: A review. *International Journal of Renewable Energy Development* **2021**, *10*, 789−802.

(4) Lin, L-Y; Ho, K.-C. Dye-Sensitized Solar Cells. *Encyclopedia of Modern Optics*; Elsevier: New York, 2018; pp 270−81.

(5) Zulkifli, A.; Iskandar, R.; Muhammad Fahmi, A. Effect of Titanium Dioxide Thickness on Performance of DSSC Solar Cell Using Red Dragon Fruit Dye. *J. Adv. Res. Fluid Mech. Thermal Sci.* **2022**, *96*, 172−81.

(6) Akila, Y.; Muthukumarasamy, N.; Velauthapillai, D. TiO2-based dye-sensitized solar cells. *Nanomaterials for Solar Cell Applications*; Elsevier: New York, 2019; pp 127−44.

(7) Gayen, R. N.; Avvaru, V. S.; Etacheri, V. Carbon-based integrated devices for efficient photo-energy conversion and storage. *Carbon Based Nanomaterials for Advanced Thermal and Electrochemical Energy Storage and Conversion*; Elsevier: New York, 2019; pp 357−74.

(8) Sai, H.; Matsui, T.; Kumagai, H.; Matsubara, K. Thin-film microcrystalline silicon solar cells: 11.9% efficiency and beyond. *Applied Physics Express* **2018**, *11*, 022301.

(9) Ramanujam, J.; Singh, U. P. Copper indium gallium selenide based solar cells − a review. *Energy Environ. Sci.* **2017**, *10*, 1306−19.

(10) Schlesinger, T. E. Gallium Arsenide. *Encyclopedia of Materials: Science and Technology*; Elsevier: New York, 2001; pp 3431−5.

(11) Sekar, R.; Ravitchandiran, A.; Angaiah, S. Recent Advances and Challenges in Light Conversion Phosphor Materials for Third-Generation Quantum-Dot-Sensitized Photovoltaics. *ACS Omega* **2022**, *7*, 35351−60.

(12) Li, Y.; Leung, W. W. Introduction of Graphene Nanofibers into the Perovskite Layer of Perovskite Solar Cells. *ChemSusChem* **2018**, *11*, 2921−9.

(13) Kanti, P. K.; Sharma, P.; Maiya, M. P.; Sharma, K. V. The stability and thermophysical properties of Al2O3-graphene oxide hybrid nanofluids for solar energy applications: Application of robust autoregressive modern machine learning technique. *Sol. Energy Mater. Sol. Cells* **2023**, *253*, 112207.

(14) Pinzón, J. R.; Villalta-Cerdas, A.; Echegoyen, L. Fullerenes, Carbon Nanotubes, and Graphene for Molecular Electronics. *Top. Curr. Chem.* **2011**, *312*, 127−174.

(15) Huang, X.; Qi, X.; Boey, F.; Zhang, H. Graphene-based composites. *Chem. Soc. Rev.* **2012**, *41*, 666−86.

(16) Fedotov, P. V.; Rybkovskiy, D. V.; Novikov, I. V.; Obraztsova, E. D. Optical Properties of 3-Armchair Graphene Nanoribbons Produced by a Combination of Chemical Vapor Deposition with a Bottom-up Approach. *Physica Status Solidi (b)* **2022**, *259*, 259.

(17) Kumar Kanti, P.; Sharma, P.; Sharma, K. V.; Maiya, M. P. The effect of pH on stability and thermal performance of graphene oxide and copper oxide hybrid nanofluids for heat transfer applications: Application of novel machine learning technique. *Journal of Energy Chemistry* **2023**, *82*, 359.

(18) Kanti, P. K.; Sharma, P.; Koneru, B.; Banerjee, P.; Jayan, K. D. Thermophysical profile of graphene oxide and MXene hybrid nanofluids for sustainable energy applications: Model prediction with a Bayesian optimized neural network with K-cross fold validation. *FlatChem.* **2023**, *39*, 100501.

(19) Huang, K.; Yin, Y.; Qu, B. Tight-binding theory of graphene mechanical properties. *Microsystem Technologies* **2021**, *27*, 3851−8.

(20) Sharma, B., Jain, P., Eds. *Graphene Based Biopolymer Nanocomposites*; Springer: Singapore, 2021.

(21) Li, X.; Wang, X.; Zhang, L.; Lee, S.; Dai, H. Chemically Derived, Ultrasmooth Graphene Nanoribbon Semiconductors. *Science (1979)* **2008**, *319*, 1229−32.

(22) Liu, F.; Qiu, X.; Xu, J.; Huang, J.; Chen, D.; Chen, G. High conductivity and transparency of graphene-based conductive ink: Prepared from a multi-component synergistic stabilization method. *Prog. Org. Coat.* **2019**, *133*, 125−30.

(23) Li, W.; Wu, W.; Li, Z. Controlling Interlayer Spacing of Graphene Oxide Membranes by External Pressure Regulation. *ACS Nano* **2018**, *12*, 9309−17.

(24) Hirsch, A. The era of carbon allotropes. *Nat. Mater.* **2010**, *9*, 868−71.

(25) Habte, A. T.; Ayele, D. W. Synthesis and Characterization of Reduced Graphene Oxide (rGO) Started from Graphene Oxide (GO) Using the Tour Method with Different Parameters. *Advances in Materials Science and Engineering* **2019**, *2019*, 1−9.

(26) Tiwari, S. K.; Sahoo, S.; Wang, N.; Huczko, A. Graphene research and their outputs: Status and prospect. *Journal of Science: Advanced Materials and Devices* **2020**, *5*, 10−29.

(27) Cao, L.; Meziani, M. J.; Sahu, S.; Sun, Y.-P. Photoluminescence Properties of Graphene versus Other Carbon Nanomaterials. *Acc. Chem. Res.* **2013**, *46*, 171−80.

(28) Shen, J.; Zhu, Y.; Yang, X.; Li, C. Graphene quantum dots: emergent nanolights for bioimaging, sensors, catalysis and photovoltaic devices. *Chem. Commun.* **2012**, *48*, 3686.

(29) Elvati, P.; Baumeister, E.; Violi, A. Graphene quantum dots: effect of size, composition and curvature on their assembly. *RSC Adv.* **2017**, *7*, 17704−17710.

(30) Yu, T.; Breslin, C. B. Review—2D Graphene and Graphene-Like Materials and Their Promising Applications in the Generation of Hydrogen Peroxide. *J. Electrochem. Soc.* **2020**, *167*, 126502.

(31) Mijatovic, D.; Eijkel, J. C. T.; van den Berg, A. Technologies for nanofluidic systems: top-down vs. bottom-up—a review. *Lab Chip* **2005**, *5*, 492.

(32) Swager, T. M. Functional Graphene: Top-Down Chemistry of the π-Surface. *ACS Macro Lett.* **2012**, *1*, 3−5.

(33) Sinclair, R. C.; Suter, J. L.; Coveney, P. V. Micromechanical exfoliation of graphene on the atomistic scale. *Phys. Chem. Chem. Phys.* **2019**, *21*, 5716−22.

(34) Cai, J.; Ruffieux, P.; Jaafar, R.; Bieri, M.; Braun, T.; Blankenburg, S.; et al. Atomically precise bottom-up fabrication of graphene nanoribbons. *Nature* **2010**, *466*, 470−3.

(35) Muñoz, R.; Gómez-Aleixandre, C. Review of <scp>CVD<scp> Synthesis of Graphene. *Chem. Vap. Deposition* **2013**, *19*, 297−322.

(36) Chaitoglou, S.; Bertran, E. Effect of temperature on graphene grown by chemical vapor deposition. *J. Mater. Sci.* **2017**, *52*, 8348−56.

(37) Kum, H.; Lee, D.; Kong, W.; Kim, H.; Park, Y.; Kim, Y.; et al. Epitaxial growth and layer-transfer techniques for heterogeneous integration of materials for electronic and photonic devices. *Nat. Electron* **2019**, *2*, 439−50.

(38) Lakshmanan, R.; Maulik, N. Graphene-based drug delivery systems in tissue engineering and nanomedicine. *Can. J. Physiol. Pharmacol.* **2018**, *96*, 869−78.

(39) Chen, X.; Qu, Z.; Du, X.; Ren, G.; Gao, Y.; Yang, Y.; et al. Mass transfer kinetics of graphene oxide prepared by chemical oxidation intercalationg assisted ultrasonic field. *Arabian Journal of Chemistry* **2023**, *16*, 104664.

(40) Patil, A. J.; Vickery, J. L.; Scott, T. B.; Mann, S. Aqueous Stabilization and Self-Assembly of Graphene Sheets into Layered Bio-Nanocomposites using DNA. *Adv. Mater.* **2009**, *21*, 3159−64.

(41) Liang, Y.; Wu, D.; Feng, X.; Müllen, K. Dispersion of Graphene Sheets in Organic Solvent Supported by Ionic Interactions. *Adv. Mater.* **2009**, *21*, 1679−83.

(42) Yang, H.; Shan, C.; Li, F.; Han, D.; Zhang, Q.; Niu, L. Covalent functionalization of polydisperse chemically-converted graphene sheets with amine-terminated ionic liquid. *Chem. Commun.* **2009**, 3880.

https://doi.org/10.1021/acsomega.3c07994
ACS Omega 2024, 9, 12403−12425

(43) Zhang, F.; Liu, F.; Wang, C.; Xin, X.; Liu, J.; Guo, S.; et al. Effect of Lateral Size of Graphene Quantum Dots on Their Properties and Application. *ACS Appl. Mater. Interfaces* **2016**, *8*, 2104−10.
(44) Zhao, W.; Suo, H.; Wang, S.; Ma, L.; Wang, L.; Wang, Q.; Zhang, Z. Mg gas infiltration for the fabrication of MgB2 pellets using nanosized and microsized B powders. *Journal of the European Ceramic Society*. **2022**, *42*, 7036.
(45) Pullagura, G.; Vanthala, V. S. P.; Vadapalli, S.; Bikkavolu, J. R.; Barik, D.; Sharma, P.; et al. Enhancing performance characteristics of biodiesel-alcohol/diesel blends with hydrogen and graphene nanoplatelets in a diesel engine. *Int. J. Hydrogen Energy* **2024**, *50*, 1020−34.
(46) Niyogi, S.; Bekyarova, E.; Itkis, M. E.; McWilliams, J. L.; Hamon, M. A.; Haddon, R. C. Solution Properties of Graphite and Graphene. *J. Am. Chem. Soc.* **2006**, *128*, 7720−1.
(47) Xu, Y.; Bai, H.; Lu, G.; Li, C.; Shi, G. Flexible Graphene Films via the Filtration of Water-Soluble Noncovalent Functionalized Graphene Sheets. *J. Am. Chem. Soc.* **2008**, *130*, 5856−7.
(48) Quintana, M.; Spyrou, K.; Grzelczak, M.; Browne, W. R.; Rudolf, P.; Prato, M. Functionalization of Graphene *via* 1,3-Dipolar Cycloaddition. *ACS Nano* **2010**, *4*, 3527−33.
(49) Ramanathan, T.; Abdala, A. A.; Stankovich, S.; Dikin, D. A.; Herrera-Alonso, M.; Piner, R. D.; et al. Functionalized graphene sheets for polymer nanocomposites. *Nat. Nanotechnol* **2008**, *3*, 327−31.
(50) Gómez-Navarro, C.; Burghard, M.; Kern, K. Elastic Properties of Chemically Derived Single Graphene Sheets. *Nano Lett.* **2008**, *8*, 2045−9.
(51) Jeon, K.-J.; Lee, Z. Size-dependent interaction of Au nanoparticles and graphene sheet. *Chem. Commun.* **2011**, *47*, 3610.
(52) Li, X.; Zhang, G.; Bai, X.; Sun, X.; Wang, X.; Wang, E.; et al. Highly conducting graphene sheets and Langmuir−Blodgett films. *Nat. Nanotechnol* **2008**, *3*, 538−42.
(53) Díez-Pascual, A. M.; Díez-Vicente, A. L. Poly(propylene fumarate)/Polyethylene Glycol-Modified Graphene Oxide Nanocomposites for Tissue Engineering. *ACS Appl. Mater. Interfaces* **2016**, *8*, 17902−14.
(54) Sharma, A.; Patel, A. K.; Bajpai, A. K.; Bajpai, R. Absorption and crystalline studies on reduced graphene oxide:poly(vinyl alcohol) polymer nano composites films. *AIP Conf. Proc.***2020**, 070001.
(55) Li, D.; Müller, M. B.; Gilje, S.; Kaner, R. B.; Wallace, G. G. Processable aqueous dispersions of graphene nanosheets. *Nat. Nanotechnol* **2008**, *3*, 101−5.
(56) Kovtyukhova, N. I.; Ollivier, P. J.; Martin, B. R.; Mallouk, T. E.; Chizhik, S. A.; Buzaneva, E. V.; et al. Layer-by-Layer Assembly of Ultrathin Composite Films from Micron-Sized Graphite Oxide Sheets and Polycations. *Chem. Mater.* **1999**, *11*, 771−8.
(57) Schedin, F.; Geim, A. K.; Morozov, S. V.; Hill, E. W.; Blake, P.; Katsnelson, M. I.; et al. Detection of individual gas molecules adsorbed on graphene. *Nat. Mater.* **2007**, *6*, 652−5.
(58) Minitha, C. R.; Anithaa, V. S.; Subramaniam, V.; Rajendra Kumar, R. T. Impact of Oxygen Functional Groups on Reduced Graphene Oxide-Based Sensors for Ammonia and Toluene Detection at Room Temperature. *ACS Omega* **2018**, *3*, 4105−12.
(59) Gao, X.; Jang, J.; Nagase, S. Hydrazine and Thermal Reduction of Graphene Oxide: Reaction Mechanisms, Product Structures, and Reaction Design. *J. Phys. Chem. C* **2010**, *114*, 832−42.
(60) Hun, S. Thermal Reduction of Graphene Oxide. *Physics and Applications of Graphene - Experiments, InTech;* **2011**.
(61) Huang, B.; Wang, Q.; Li, Y.; Zhang, M.; Wei, X. Preparation and characterisation of graphene. *Materials Research Innovations* **2015**, *19*, S9-344−S9-350.
(62) Novoselov, K. S.; Geim, A. K.; Morozov, S. V.; Jiang, D.; Zhang, Y.; Dubonos, S. V.; et al. Electric Field Effect in Atomically Thin Carbon Films. *Science (1979)* **2004**, *306*, 666−9.
(63) Morozov, S. V.; Novoselov, K. S.; Katsnelson, M. I.; Schedin, F.; Elias, D. C.; Jaszczak, J. A.; et al. Giant Intrinsic Carrier Mobilities in Graphene and Its Bilayer. *Phys. Rev. Lett.* **2008**, *100*, 016602.
(64) Bolotin, K. I.; Sikes, K. J.; Jiang, Z.; Klima, M.; Fudenberg, G.; Hone, J.; et al. Ultrahigh electron mobility in suspended graphene. *Solid State Commun.* **2008**, *146*, 351−5.
(65) Yan, K.; Fu, L.; Peng, H.; Liu, Z. Designed CVD Growth of Graphene via Process Engineering. *Acc. Chem. Res.* **2013**, *46*, 2263−74.
(66) Balandin, A. A.; Ghosh, S.; Bao, W.; Calizo, I.; Teweldebrhan, D.; Miao, F.; et al. Superior Thermal Conductivity of Single-Layer Graphene. *Nano Lett.* **2008**, *8*, 902−7.
(67) Hong, T.-K.; Lee, D. W.; Choi, H. J.; Shin, H. S.; Kim, B.-S. Transparent, Flexible Conducting Hybrid Multilayer Thin Films of Multiwalled Carbon Nanotubes with Graphene Nanosheets. *ACS Nano* **2010**, *4*, 3861−8.
(68) Wassei, J. K.; Kaner, R. B. Graphene, a promising transparent conductor. *Mater. Today* **2010**, *13*, 52−9.
(69) Leenaerts, O.; Peelaers, H.; Hernández-Nieves, A. D.; Partoens, B.; Peeters, F. M. First-principles investigation of graphene fluoride and graphane. *Phys. Rev. B* **2010**, *82*, 195436.
(70) Thirumurugan, A.; Udayabhaskar, R.; Prabhakaran, T.; Morel, M. J.; Akbari-Fakhrabadi, A.; Ravichandran, K.; et al. Magnetic and electrochemical characteristics of carbon-modified magnetic nanoparticles. *Fundamentals and Properties of Multifunctional Nanomaterials*; Elsevier: New York, 2021; pp 235−52.
(71) Sharma, A.; Das, S.; Das, K. Pulse Electrodeposition of Lead-Free Tin-Based Composites for Microelectronic Packaging. *Electrodeposition of Composite Materials, InTech;* **2016**.
(72) Jung, D. Y.; Yang, S. Y.; Park, H.; Shin, W. C.; Oh, J. G.; Cho, B. J.; et al. Interface engineering for high performance graphene electronic devices. *Nano Converg* **2015**, *2*, 11.
(73) Mahmoudi, T.; Wang, Y.; Hahn, Y.-B. Graphene and its derivatives for solar cells application. *Nano Energy* **2018**, *47*, 51−65.
(74) Biria, S.; Chen, F.; Hosein, I. D. Enhanced Wide-Angle Energy Conversion Using Structure-Tunable Waveguide Arrays as Encapsulation Materials for Silicon Solar Cells. *Physica Status Solidi (a)* **2019**, *216*, 216.
(75) Bacon, M.; Bradley, S. J.; Nann, T. Graphene Quantum Dots. *Particle & Particle Systems Characterization* **2014**, *31*, 415−28.
(76) Zhao, J.; Wu, J.; Zheng, M.; Huo, J.; Tu, Y. Improving the photovoltaic performance of dye-sensitized solar cell by graphene/titania photoanode. *Electrochim. Acta* **2015**, *156*, 261−6.
(77) Sharma, D.; Jha, R.; Kumar, S. Quantum dot sensitized solar cell: Recent advances and future perspectives in photoanode. *Sol. Energy Mater. Sol. Cells* **2016**, *155*, 294−322.
(78) Yang, N.; Zhai, J.; Wang, D.; Chen, Y.; Jiang, L. Two-Dimensional Graphene Bridges Enhanced Photoinduced Charge Transport in Dye-Sensitized Solar Cells. *ACS Nano* **2010**, *4*, 887−94.
(79) Kumar, S.; McEvoy, N.; Kim, H.; Lee, K.; Peltekis, N.; Rezvani, E.; et al. CVD growth and processing of graphene for electronic applications. *Physica Status Solidi (b)* **2011**, *248*, 2604−8.
(80) Arif, T.; Colas, G.; Filleter, T. Effect of Humidity and Water Intercalation on the Tribological Behavior of Graphene and Graphene Oxide. *ACS Appl. Mater. Interfaces* **2018**, *10*, 22537−44.
(81) Annett, J.; Cross, G. L. W. Self-assembly of graphene ribbons by spontaneous self-tearing and peeling from a substrate. *Nature* **2016**, *535*, 271−5.
(82) Kozlova, M.; Butrim, S.; Solovyev, M.; Pushkarev, A.; Pushkareva, I.; Kalinichenko, V.; et al. Structural and Electrochemical Characteristics of Platinum Nanoparticles Supported on Various Carbon Carriers. *C (Basel)* **2022**, *8*, 14.
(83) Zhang, X.; Tang, Y.; Zhang, F.; Lee, C. A Novel Aluminum-Graphite Dual-Ion Battery. *Adv. Energy Mater.* **2016**, *6* (11), 1502588.
(84) Chen, J.; Zhang, Z.; Lu, H. Structure design and properties investigation of Bi2O2Se/graphene van der Waals heterojunction from first-principles study. *Surfaces and Interfaces* **2022**, *33*, 102289.
(85) Subrahmanyam, K. S.; Panchakarla, L. S.; Govindaraj, A.; Rao, C. N. R. Simple Method of Preparing Graphene Flakes by an Arc-Discharge Method. *J. Phys. Chem. C* **2009**, *113*, 4257−9.

https://doi.org/10.1021/acsomega.3c07994
ACS Omega 2024, 9, 12403−12425

(86) Chen, W.; Yan, L.; Bangal, P. R. Preparation of graphene by the rapid and mild thermal reduction of graphene oxide induced by microwaves. *Carbon N Y* **2010**, *48*, 1146−52.
(87) Li, X.; Aftab, S.; Abbas, A.; Hussain, S.; Aslam, M.; Kabir, F.; Ansari, M. Z. Advances in mixed 2D and 3D perovskite heterostructure solar cells: A comprehensive review. *Nano Energy* **2023**, *118*, 108979.
(88) Kim, C.-D.; Min, B.-K.; Jung, W.-S. Preparation of graphene sheets by the reduction of carbon monoxide. *Carbon N Y* **2009**, *47*, 1610−2.
(89) Gürünlü, B.; Tasdelen-Yücedag, Ç; Bayramoglu, M. Graphene Synthesis by Ultrasound Energy-Assisted Exfoliation of Graphite in Various Solvents. *Crystals (Basel)* **2020**, *10*, 1037.
(90) Cui, X.; Zhang, C.; Hao, R.; Hou, Y. Liquid-phase exfoliation, functionalization and applications of graphene. *Nanoscale* **2011**, *3*, 2118.
(91) Qiu, Y.; Shi, M.; Guo, X.; Li, J.; Wu, J.; Zhou, Y.; Li, Y. Sensitivity improvement in the measurement of minor components by spatial confinement in fiber-optic laser-induced breakdown spectroscopy. *Spectrochimica Acta Part B: Atomic Spectroscopy* **2023**, *209*, 106800.
(92) Book, K.; Bässler, H.; Elschner, A.; Kirchmeyer, S. Hole injection from an ITO|PEDT anode into the hole transporting layer of an OLED probed by bias induced absorption. *Org. Electron* **2003**, *4*, 227−32.
(93) Park, J.-H.; Kang, S. J.; Na, S.-I.; Lee, H. H.; Kim, S.-W.; Hosono, H.; et al. Indium-free, acid-resistant anatase Nb-doped TiO2 electrodes activated by rapid-thermal annealing for cost-effective organic photovoltaics. *Sol. Energy Mater. Sol. Cells* **2011**, *95*, 2178−85.
(94) Zou, Y.; Zhong, M.; Li, S.; Qing, Z.; Xing, X.; Gong, G.; Zhou, C. Flexible Wearable Strain Sensors Based on Laser-Induced Graphene for Monitoring Human Physiological Signals. *Polymers* **2023**, *15* (17), 3553.
(95) Pitchaiya, S.; Natarajan, M.; Santhanam, A.; Asokan, V.; Yuvapragasam, A.; Madurai Ramakrishnan, V.; et al. A review on the classification of organic/inorganic/carbonaceous hole transporting materials for perovskite solar cell application. *Arabian Journal of Chemistry* **2020**, *13*, 2526−57.
(96) Liu, Z.; Li, J.; Yan, F. Package-Free Flexible Organic Solar Cells with Graphene top Electrodes. *Adv. Mater.* **2013**, *25*, 4296−301.
(97) Du, S.; Xie, H.; Yin, J.; Sun, Y.; Wang, Q.; Liu, H.; Zheng, R. Giant hot electron thermalization via stacking of graphene layers. *Carbon* **2023**, *203* (25), 835−841.
(98) Yin, Z.; Wu, S.; Zhou, X.; Huang, X.; Zhang, Q.; Boey, F.; et al. Electrochemical Deposition of ZnO Nanorods on Transparent Reduced Graphene Oxide Electrodes for Hybrid Solar Cells. *Small* **2010**, *6*, 307−12.
(99) Park, J.-H.; Ahn, K.-J.; Na, S.-I.; Kim, H.-K. Effects of deposition temperature on characteristics of Ga-doped ZnO film prepared by highly efficient cylindrical rotating magnetron sputtering for organic solar cells. *Sol. Energy Mater. Sol. Cells* **2011**, *95*, 657−63.
(100) Wang, J.; Xie, Z.; Yeow, J. T. W. Review—State-of-the-Art Organic Solar Cells based on Carbon Nanotubes and Graphene. *ECS Journal of Solid State Science and Technology* **2020**, *9*, 105004.
(101) Du, S.; Yin, J.; Xie, H.; Sun, Y.; Fang, T.; Wang, Y.; Zheng, R. Auger scattering dynamic of photo-excited hot carriers in nano-graphite film. *Appl. Phys. Lett.* **2022**, *121*, 181104.
(102) Ali, A. Y.; Holmes, N. P.; Ameri, M.; Feron, K.; Thameel, M. N.; Barr, M. G.; et al. Low-Temperature CVD-Grown Graphene Thin Films as Transparent Electrode for Organic Photovoltaics. *Coatings* **2022**, *12*, 681.
(103) Wu, J.; Becerril, H. A.; Bao, Z.; Liu, Z.; Chen, Y.; Peumans, P. Organic solar cells with solution-processed graphene transparent electrodes. *Appl. Phys. Lett.* **2008**, *92*, 92.
(104) Lan, G.; Tang, L.; Dong, J.; Nong, J.; Luo, P.; Li, X.; Wei, W. Enhanced Asymmetric Light-Plasmon Coupling in Graphene Nanoribbons for High-Efficiency Transmissive Infrared Modulation. *Laser & Photonics Reviews.* **2024**.
(105) Sun, Y.; Zhang, W.; Chi, H.; Liu, Y.; Hou, C. L.; Fang, D. Recent development of graphene materials applied in polymer solar cell. *Renewable and Sustainable Energy Reviews* **2015**, *43*, 973−80.
(106) Han, X.; Chen, Y.; Zhu, H.; Preston, C.; Wan, J.; Fang, Z.; et al. Scalable, printable, surfactant-free graphene ink directly from graphite. *Nanotechnology* **2013**, *24*, 205304.
(107) Romero, H. E.; Shen, N.; Joshi, P.; Gutierrez, H. R.; Tadigadapa, S. A.; Sofo, J. O.; et al. n-Type Behavior of Graphene Supported on Si/SiO $_2$ Substrates. *ACS Nano* **2008**, *2*, 2037−44.
(108) Wang, J.; Zhang, Y.; Liu, G.; Zhang, T.; Zhang, C.; Zhang, Y.; Chi, Q. Improvements in the Magnesium Ion Transport Properties of Graphene/CNT-wrapped TiO2-B Nanoflowers by Nickel Doping. *Small* **2024**.
(109) Charlier, J.-C.; Blase, X.; Roche, S. Electronic and transport properties of nanotubes. *Rev. Mod. Phys.* **2007**, *79*, 677−732.
(110) Ma, K. L.; Yan, X. H.; Guo, Y. D.; Xiao, Y. Electronic transport properties of junctions between carbon nanotubes and graphene nanoribbons. *Eur. Phys. J. B* **2011**, *83*, 487−92.
(111) Chen, L.; Zhao, Y.; Li, M.; Li, L.; Hou, L.; Hou, H. Reinforced AZ91D magnesium alloy with thixomolding process facilitated dispersion of graphene nanoplatelets and enhanced interfacial interactions. *Materials Science and Engineering: A* **2021**, *804*, 140793.
(112) Bégué, D.; Guille, E.; Metz, S.; Arnaud, M. A.; Silva, H. S.; Seck, M.; et al. Graphene-based acceptor molecules for organic photovoltaic cells: a predictive study identifying high modularity and morphological stability. *RSC Adv.* **2016**, *6*, 13653−6.
(113) Li, M.; Guo, Q.; Chen, L.; Li, L.; Hou, H.; Zhao, Y. Microstructure and properties of graphene nanoplatelets reinforced AZ91D matrix composites prepared by electromagnetic stirring casting. *Journal of Materials Research and Technology* **2022**, *21*, 4138−4150.
(114) Mahmoudi, T.; Seo, S.; Yang, H.-Y.; Rho, W.-Y.; Wang, Y.; Hahn, Y.-B. Efficient bulk heterojunction hybrid solar cells with graphene-silver nanoparticles composite synthesized by microwave-assisted reduction. *Nano Energy* **2016**, *28*, 179−87.
(115) Chu, T.-Y.; Lu, J.; Beaupré, S.; Zhang, Y.; Pouliot, J.-R.; Wakim, S.; et al. Bulk Heterojunction Solar Cells Using Thieno[3,4-*c*]pyrrole-4,6-dione and Dithieno[3,2- *b* :2′,3′- *d*]silole Copolymer with a Power Conversion Efficiency of 7.3%. *J. Am. Chem. Soc.* **2011**, *133*, 4250−3.
(116) Yan, Z.; Hu, Q.; Jiang, F.; Lin, S.; Li, R.; Chen, S. Mechanism and technology evaluation of a novel alternating-arc-based directed energy deposition method through polarity-switching self-adaptive shunt. *Additive Manufacturing* **2023**, *67*, 103504.
(117) Mahmoudi, T.; Rho, W.-Y.; Yang, H.-Y.; Silva, S. R. P.; Hahn, Y.-B. Highly conductive and dispersible graphene and its application in P3HT-based solar cells. *Chem. Commun.* **2014**, *50*, 8705.
(118) He, Z.; Zhong, C.; Huang, X.; Wong, W.; Wu, H.; Chen, L.; et al. Simultaneous Enhancement of Open-Circuit Voltage, Short-Circuit Current Density, and Fill Factor in Polymer Solar Cells. *Adv. Mater.* **2011**, *23*, 4636−43.
(119) Feng, J.; Dong, H.; Pang, B.; Shao, F.; Zhang, C.; Yu, L.; et al. Theoretical study on the optical and electronic properties of graphene quantum dots doped with heteroatoms. *Phys. Chem. Chem. Phys.* **2018**, *20*, 15244−52.
(120) Van Le, Q.; Choi, J.-Y.; Kim, S. Y. Recent advances in the application of two-dimensional materials as charge transport layers in organic and perovskite solar cells. *FlatChem.* **2017**, *2*, 54−66.
(121) Mahala, P.; Gupta, N.; Singh, S. Silicon photovoltaic cell based on graphene oxide as an active layer. *Microsystem Technologies* **2021**, *27*, 4027−33.
(122) Yip, H.; Hau, S. K.; Baek, N. S.; Ma, H.; Jen, AK -Y Polymer Solar Cells That Use Self-Assembled-Monolayer- Modified ZnO/Metals as Cathodes. *Adv. Mater.* **2008**, *20*, 2376−82.
(123) Lv, F.; Ma, Y.; Xiang, P.; Shu, T.; Tan, X.; Qiu, L.; et al. N-I co-doped TiO2 compact film as a highly effective n-type electron blocking layer for solar cells. *J. Alloys Compd.* **2020**, *837*, 155555.
(124) Yang, Y.; Han, C.; Jiang, B.; Iocozzia, J.; He, C.; Shi, D.; et al. Graphene-based materials with tailored nanostructures for energy

https://doi.org/10.1021/acsomega.3c07994
ACS Omega 2024, 9, 12403−12425

conversion and storage. *Materials Science and Engineering: R: Reports* **2016**, *102*, 1−72.
(125) Woo Lee, H.; Young Oh, J.; Lee, T.; Soon Jang, W.; Bum Yoo, Y.; Sang Chae, S.; et al. Highly efficient inverted polymer solar cells with reduced graphene-oxide-zinc-oxide nanocomposites buffer layer. *Appl. Phys. Lett.* **2013**, 102.
(126) Wang, D. H.; Kim, J. K.; Seo, J. H.; Park, I.; Hong, B. H.; Park, J. H.; et al. Transferable Graphene Oxide by Stamping Nanotechnology: Electron-Transport Layer for Efficient Bulk-Heterojunction Solar Cells. *Angew. Chem., Int. Ed.* **2013**, *52*, 2874−80.
(127) Satapathi, S.; Gill, H. S.; Das, S.; Li, L.; Samuelson, L.; Green, M. J.; et al. Performance enhancement of dye-sensitized solar cells by incorporating graphene sheets of various sizes. *Appl. Surf. Sci.* **2014**, *314*, 638−41.
(128) Younas, M.; Baroud, T. N.; Gondal, M. A.; Dastageer, M. A.; Giannelis, E. P. Highly efficient, cost-effective counter electrodes for dye-sensitized solar cells (DSSCs) augmented by highly mesoporous carbons. *J. Power Sources* **2020**, *468*, 228359.
(129) Paulo, S.; Palomares, E.; Martinez-Ferrero, E. Graphene and Carbon Quantum Dot-Based Materials in Photovoltaic Devices: From Synthesis to Applications. *Nanomaterials* **2016**, *6*, 157.
(130) Cho, H.-H.; Cho, C.-H.; Kang, H.; Yu, H.; Oh, J. H.; Kim, B. J. Molecular structure-device performance relationship in polymer solar cells based on indene-C60 bis-adduct derivatives. *Korean Journal of Chemical Engineering* **2015**, *32*, 261−7.
(131) Zheng, H.; Neo, C. Y.; Ouyang, J. Highly Efficient Iodide/Triiodide Dye-Sensitized Solar Cells with Gel-Coated Reduce Graphene Oxide/Single-Walled Carbon Nanotube Composites as the Counter Electrode Exhibiting an Open-Circuit Voltage of 0.90 V. *ACS Appl. Mater. Interfaces* **2013**, *5*, 6657−64.
(132) Neo, C. Y.; Ouyang, J. The production of organogels using graphene oxide as the gelator for use in high-performance quasi-solid state dye-sensitized solar cells. *Carbon N Y* **2013**, *54*, 48−57.
(133) Yen, M.-Y.; Hsiao, M.-C.; Liao, S.-H.; Liu, P.-I.; Tsai, H.-M.; Ma, C-CM; et al. Preparation of graphene/multi-walled carbon nanotube hybrid and its use as photoanodes of dye-sensitized solar cells. *Carbon N Y* **2011**, *49*, 3597−606.
(134) Verduci, R.; Agresti, A.; Romano, V.; D'Angelo, G. Interface Engineering for Perovskite Solar Cells Based on 2D-Materials: A Physics Point of View. *Materials* **2021**, *14*, 5843.
(135) Wang, Y.; Mahmoudi, T.; Rho, W.-Y.; Yang, H.-Y.; Seo, S.; Bhat, K. S.; et al. Ambient-air-solution-processed efficient and highly stable perovskite solar cells based on CH3NH3PbI3−xClx-NiO composite with Al2O3/NiO interfacial engineering. *Nano Energy* **2017**, *40*, 408−17.
(136) Wang, Y.; Rho, W.-Y.; Yang, H.-Y.; Mahmoudi, T.; Seo, S.; Lee, D.-H.; et al. Air-stable, hole-conductor-free high photocurrent perovskite solar cells with CH3NH3PbI3−NiO nanoparticles composite. *Nano Energy* **2016**, *27*, 535−44.
(137) Su, H.; Wu, T.; Cui, D.; Lin, X.; Luo, X.; Wang, Y.; et al. The Application of Graphene Derivatives in Perovskite Solar Cells. *Small Methods* **2020**, *4*, 4.
(138) You, J.; Hong, Z.; Yang, Y.; Chen, Q.; Cai, M.; Song, T.-B.; et al. Low-Temperature Solution-Processed Perovskite Solar Cells with High Efficiency and Flexibility. *ACS Nano* **2014**, *8*, 1674−80.
(139) Liu, X.; Yu, H.; Yan, L.; Dong, Q.; Wan, Q.; Zhou, Y.; et al. Triple Cathode Buffer Layers Composed of PCBM, C_{60}, and LiF for High-Performance Planar Perovskite Solar Cells. *ACS Appl. Mater. Interfaces* **2015**, *7*, 6230−7.
(140) Bai, Y.; Yu, H.; Zhu, Z.; Jiang, K.; Zhang, T.; Zhao, N.; et al. High performance inverted structure perovskite solar cells based on a PCBM:polystyrene blend electron transport layer. *J. Mater. Chem. A Mater.* **2015**, *3*, 9098−102.
(141) Bhowmik, A.; Kumar, R.; Babbar, A.; Romanovski, V.; Roy, S.; Patnaik, L.; Kumar, J. P.; Alawadi, A. H. Analysis of physical, mechanical and tribological behavior of Al7075-fly ash composite for lightweight applications. *International Journal on Interactive Design and Manufacturing (IJIDeM)* **2023**, 1−14.
(142) Kuang, C.; Tang, G.; Jiu, T.; Yang, H.; Liu, H.; Li, B.; et al. Highly Efficient Electron Transport Obtained by Doping PCBM with Graphdiyne in Planar-Heterojunction Perovskite Solar Cells. *Nano Lett.* **2015**, *15*, 2756−62.
(143) Adam, G.; Kaltenbrunner, M.; Głowacki, E. D.; Apaydin, D. H.; White, M. S.; Heilbrunner, H.; et al. Solution processed perovskite solar cells using highly conductive PEDOT:PSS interfacial layer. *Sol. Energy Mater. Sol. Cells* **2016**, *157*, 318−25.
(144) Kour, K.; Badogu, K.; Babbar, A.; Sood, A.; Kumar, R.; Singh, G. On melt flow and wear properties of recycled Nylon 6-Zirconia composites for 3D printing in rapid tooling applications. *Mater. Today: Proc.* **2023**, 1 DOI: 10.1016/j.matpr.2023.10.029.
(145) Tavakoli, M. M.; Tavakoli, R.; Hasanzadeh, S.; Mirfasih, M. H. Interface Engineering of Perovskite Solar Cell Using a Reduced-Graphene Scaffold. *J. Phys. Chem. C* **2016**, *120*, 19531−6.
(146) Zhou, Y.; Yang, S.; Yin, X.; Han, J.; Tai, M.; Zhao, X.; et al. Enhancing electron transport *via* graphene quantum dot/SnO_2 composites for efficient and durable flexible perovskite photovoltaics. *J. Mater. Chem. A Mater.* **2019**, *7*, 1878−88.
(147) Babbar, A.; Jain, V.; Gupta, D.; Prakash, C. Experimental investigation and parametric optimization of neurosurgical bone grinding under bio-mimic environment. *Surf. Rev. Lett.* **2023**, *30* (01), 2141005.
(148) Safie, N. E.; Azam, M. A.; Aziz, M. F. A.; Ismail, M. Recent progress of graphene-based materials for efficient charge transfer and device performance stability in perovskite solar cells. *Int. J. Energy Res.* **2021**, *45*, 1347−74.
(149) Raja, R.; Govindaraj, M.; Antony, M. D.; Krishnan, K.; Velusamy, E.; Sambandam, A.; et al. Effect of TiO2/reduced graphene oxide composite thin film as a blocking layer on the efficiency of dye-sensitized solar cells. *J. Solid State Electrochem.* **2017**, *21*, 891−903.
(150) Kumar, A.; Babbar, A.; Jain, V.; Gupta, D.; Pathri, B. P.; Prakash, C.; Saxena, K. K.; Kumar, S. Investigation and enhancement of mechanical properties of SS-316 weldment using TiO2-SiO2-Al2O3 hybrid flux. *International Journal on Interactive Design and Manufacturing (IJIDeM)* **2023**, 1−17.
(151) Motlak, M.; Barakat, N. A. M.; Akhtar, M. S.; El-Deen, A. G.; Obaid, M.; Kim, C. S.; et al. High-efficiency dye-sensitized solar cells based on nitrogen and graphene oxide co-incorporated TiO2 nanofibers photoelectrode. *Chemical Engineering Journal* **2015**, *268*, 153−61.
(152) Babbar, A.; Jain, V.; Gupta, D.; Goyal, K. K.; Prakash, C.; Saxena, K. K.; Kumar, S.; Bartoszuk, M. Investigation of infrared thermography of cortical bone grinding in neurosurgery. *Advances in Science and Technology Research Journal* **2023**, *17* (1), 116−123.
(153) Bell, N. J.; Ng, Y. H.; Du, A.; Coster, H.; Smith, S. C.; Amal, R. Understanding the Enhancement in Photoelectrochemical Properties of Photocatalytically Prepared TiO_2 -Reduced Graphene Oxide Composite. *J. Phys. Chem. C* **2011**, *115*, 6004−9.
(154) Tayebi, M.; Kolaei, M.; Tayyebi, A.; Masoumi, Z.; Belbasi, Z.; Lee, B.-K. Reduced graphene oxide (RGO) on TiO2 for an improved photoelectrochemical (PEC) and photocatalytic activity. *Sol. Energy* **2019**, *190*, 185−94.
(155) Nan, H. Y.; Ni, Z. H.; Wang, J.; Zafar, Z.; Shi, Z. X.; Wang, Y. Y. The thermal stability of graphene in air investigated by Raman spectroscopy. *J. Raman Spectrosc.* **2013**, *44*, 1018−21.
(156) Aryal, U. K.; Ahmadpour, M.; Turkovic, V.; Rubahn, H.-G.; Di Carlo, A.; Madsen, M. 2D materials for organic and perovskite photovoltaics. *Nano Energy* **2022**, *94*, 106833.
(157) Babbar, A., Sharma, A., Jain, V., Gupta, D., Eds. *Additive Manufacturing Processes in Biomedical Engineering: Advanced Fabrication Methods and Rapid Tooling Techniques*; CRC Press: New York, 2022.
(158) Fang, H.; Chuang, S.; Chang, T. C.; Takei, K.; Takahashi, T.; Javey, A. High-Performance Single Layered WSe_2 p-FETs with Chemically Doped Contacts. *Nano Lett.* **2012**, *12*, 3788−92.
(159) Xia, F.; Wang, H.; Jia, Y. Rediscovering black phosphorus as an anisotropic layered material for optoelectronics and electronics. *Nat. Commun.* **2014**, *5*, 4458.

https://doi.org/10.1021/acsomega.3c07994
ACS Omega 2024, 9, 12403−12425

(160) Akinwande, D.; Brennan, C. J.; Bunch, J. S.; Egberts, P.; Felts, J. R.; Gao, H.; et al. A review on mechanics and mechanical properties of 2D materials—Graphene and beyond. *Extreme Mech Lett.* **2017**, *13*, 42−77.
(161) Liu, K.; Wu, J. Mechanical properties of two-dimensional materials and heterostructures. *J. Mater. Res.* **2016**, *31*, 832−44.
(162) Li, X.; Sun, M.; Wei, X.; Shan, C.; Chen, Q. 1D Piezoelectric Material Based Nanogenerators: Methods, Materials and Property Optimization. *Nanomaterials* **2018**, *8*, 188.
(163) Kedzierski, T.; Baranowska, D.; Beben, D.; Zielińska, B.; Chen, X.; Mijowska, E. Flexible Films as Anode Materials Based on rGO and TiO2/MnO2 in Li-Ion Batteries Free of Non-Active Agents. *Energies (Basel)* **2021**, *14*, 8168.
(164) Han, G. S.; Chung, H. S.; Kim, B. J.; Kim, D. H.; Lee, J. W.; Swain, B. S.; et al. Retarding charge recombination in perovskite solar cells using ultrathin MgO-coated TiO_2 nanoparticulate films. *J. Mater. Chem. A Mater.* **2015**, *3*, 9160−4.
(165) Cho, K. T.; Grancini, G.; Lee, Y.; Konios, D.; Paek, S.; Kymakis, E.; et al. Beneficial Role of Reduced Graphene Oxide for Electron Extraction in Highly Efficient Perovskite Solar Cells. *ChemSusChem* **2016**, *9*, 3040−4.
(166) Xie, J.; Huang, K.; Yu, X.; Yang, Z.; Xiao, K.; Qiang, Y.; et al. Enhanced Electronic Properties of SnO_2 *via* Electron Transfer from Graphene Quantum Dots for Efficient Perovskite Solar Cells. *ACS Nano* **2017**, *11*, 9176−82.
(167) Jeon, I.; Yoon, J.; Ahn, N.; Atwa, M.; Delacou, C.; Anisimov, A.; et al. Carbon Nanotubes versus Graphene as Flexible Transparent Electrodes in Inverted Perovskite Solar Cells. *J. Phys. Chem. Lett.* **2017**, *8*, 5395−401.
(168) Feng, S.; Yang, Y.; Li, M.; Wang, J.; Cheng, Z.; Li, J.; et al. High-Performance Perovskite Solar Cells Engineered by an Ammonia Modified Graphene Oxide Interfacial Layer. *ACS Appl. Mater. Interfaces* **2016**, *8*, 14503−12.
(169) Yoon, J.; Sung, H.; Lee, G.; Cho, W.; Ahn, N.; Jung, H. S.; et al. Superflexible, high-efficiency perovskite solar cells utilizing graphene electrodes: towards future foldable power sources. *Energy Environ. Sci.* **2017**, *10*, 337−45.
(170) Agresti, A.; Pescetelli, S.; Palma, A. L.; Del Rio Castillo, A. E.; Konios, D.; Kakavelakis, G.; et al. Graphene Interface Engineering for Perovskite Solar Modules: 12.6% Power Conversion Efficiency over 50 cm^2 Active Area. *ACS Energy Lett.* **2017**, *2*, 279−87.
(171) Li, J.; Qiu, Y.; Wei, Z.; Lin, Q.; Zhang, Q.; Yan, K.; et al. A three-dimensional hexagonal fluorine-doped tin oxide nanocone array: a superior light harvesting electrode for high performance photo-electrochemical water splitting. *Energy Environ. Sci.* **2014**, *7*, 3651−8.
(172) You, P.; Liu, Z.; Tai, Q.; Liu, S.; Yan, F. Efficient Semitransparent Perovskite Solar Cells with Graphene Electrodes. *Adv. Mater.* **2015**, *27*, 3632−8.
(173) Du, P.; Hu, X.; Yi, C.; Liu, H. C.; Liu, P.; Zhang, H.; et al. Self-Powered Electronics by Integration of Flexible Solid-State Graphene-Based Supercapacitors with High Performance Perovskite Hybrid Solar Cells. *Adv. Funct Mater.* **2015**, *25*, 2420−7.
(174) Ye, S.; Rao, H.; Yan, W.; Li, Y.; Sun, W.; Peng, H.; et al. A Strategy to Simplify the Preparation Process of Perovskite Solar Cells by Co-deposition of a Hole-Conductor and a Perovskite Layer. *Adv. Mater.* **2016**, *28*, 9648−54.
(175) Palma, A. L.; Cinà, L.; Pescetelli, S.; Agresti, A.; Raggio, M.; Paolesse, R.; et al. Reduced graphene oxide as efficient and stable hole transporting material in mesoscopic perovskite solar cells. *Nano Energy* **2016**, *22*, 349−60.
(176) Yoshikawa, K.; Kawasaki, H.; Yoshida, W.; Irie, T.; Konishi, K.; Nakano, K.; et al. Silicon heterojunction solar cell with interdigitated back contacts for a photoconversion efficiency over 26%. *Nat. Energy* **2017**, *2*, 17032.
(177) Chung, C.-C.; Narra, S.; Jokar, E.; Wu, H.-P.; Wei-Guang Diau, E. Inverted planar solar cells based on perovskite/graphene oxide hybrid composites. *J. Mater. Chem. A Mater.* **2017**, *5*, 13957−65.
(178) Hadadian, M.; Correa-Baena, J.; Goharshadi, E. K.; Ummadisingu, A.; Seo, J.; Luo, J.; et al. Enhancing Efficiency of Perovskite Solar Cells via N-doped Graphene: Crystal Modification and Surface Passivation. *Adv. Mater.* **2016**, *28*, 8681−6.
(179) Fang, X.; Ding, J.; Yuan, N.; Sun, P.; Lv, M.; Ding, G.; et al. Graphene quantum dot incorporated perovskite films: passivating grain boundaries and facilitating electron extraction. *Phys. Chem. Chem. Phys.* **2017**, *19*, 6057−63.
(180) Chen, H.; Luo, Q.; Liu, T.; Tai, M.; Lin, J.; Murugadoss, V.; et al. Boosting Multiple Interfaces by Co-Doped Graphene Quantum Dots for High Efficiency and Durability Perovskite Solar Cells. *ACS Appl. Mater. Interfaces* **2020**, *12*, 13941−9.
(181) Agresti, A.; Pescetelli, S.; Taheri, B.; Del Rio Castillo, A. E.; Cinà, L.; Bonaccorso, F.; et al. Graphene−Perovskite Solar Cells Exceed 18% Efficiency: A Stability Study. *ChemSusChem* **2016**, *9*, 2609−19.
(182) Biccari, F.; Gabelloni, F.; Burzi, E.; Gurioli, M.; Pescetelli, S.; Agresti, A.; et al. Graphene-Based Electron Transport Layers in Perovskite Solar Cells: A Step-Up for an Efficient Carrier Collection. *Adv. Energy Mater.* **2017**, *7*, 7.
(183) O'Keeffe, P.; Catone, D.; Paladini, A.; Toschi, F.; Turchini, S.; Avaldi, L.; et al. Graphene-Induced Improvements of Perovskite Solar Cell Stability: Effects on Hot-Carriers. *Nano Lett.* **2019**, *19*, 684−91.
(184) Li, H.; Shi, W.; Huang, W.; Yao, E.-P.; Han, J.; Chen, Z.; et al. Carbon Quantum Dots/TiO_x Electron Transport Layer Boosts Efficiency of Planar Heterojunction Perovskite Solar Cells to 19%. *Nano Lett.* **2017**, *17*, 2328−35.
(185) Cho, K. T.; Grancini, G.; Lee, Y.; Konios, D.; Paek, S.; Kymakis, E.; et al. Beneficial Role of Reduced Graphene Oxide for Electron Extraction in Highly Efficient Perovskite Solar Cells. *ChemSusChem* **2016**, *9*, 3040−4.
(186) Patil, J. V.; Mali, S. S.; Patil, A. P.; Patil, P. S.; Hong, C. K. Highly efficient mixed-halide mixed-cation perovskite solar cells based on rGO-TiO2 composite nanofibers. *Energy* **2019**, *189*, 116396.
(187) Agresti, A.; Pescetelli, S.; Cinà, L.; Konios, D.; Kakavelakis, G.; Kymakis, E.; et al. Efficiency and Stability Enhancement in Perovskite Solar Cells by Inserting Lithium-Neutralized Graphene Oxide as Electron Transporting Layer. *Adv. Funct Mater.* **2016**, *26*, 2686−94.
(188) Nouri, E.; Mohammadi, M. R.; Lianos, P. Improving the stability of inverted perovskite solar cells under ambient conditions with graphene-based inorganic charge transporting layers. *Carbon N Y* **2018**, *126*, 208−14.
(189) Chandrasekhar, P. S.; Komarala, V. K. Graphene/ZnO nanocomposite as an electron transport layer for perovskite solar cells; the effect of graphene concentration on photovoltaic performance. *RSC Adv.* **2017**, *7*, 28610−5.
(190) Chandrasekhar, P. S.; Dubey, A.; Qiao, Q. High efficiency perovskite solar cells using nitrogen-doped graphene/ZnO nanorod composite as an electron transport layer. *Sol. Energy* **2020**, *197*, 78−83.
(191) Tavakoli, M. M.; Tavakoli, R.; Yadav, P.; Kong, J. A graphene/ZnO electron transfer layer together with perovskite passivation enables highly efficient and stable perovskite solar cells. *J. Mater. Chem. A Mater.* **2019**, *7*, 679−86.
(192) Zhu, M.; Liu, W.; Ke, W.; Xie, L.; Dong, P.; Hao, F. Graphene-Modified Tin Dioxide for Efficient Planar Perovskite Solar Cells with Enhanced Electron Extraction and Reduced Hysteresis. *ACS Appl. Mater. Interfaces* **2019**, *11*, 666−73.
(193) Liu, X.; Yang, X.; Liu, X.; Zhao, Y.; Chen, J.; Gu, Y. High efficiency flexible perovskite solar cells using SnO2/graphene electron selective layer and silver nanowires electrode. *Appl. Phys. Lett.* **2018**, *113*, 113.
(194) Hong, J. A.; Jung, E. D.; Yu, J. C.; Kim, D. W.; Nam, Y. S.; Oh, I.; et al. Improved Efficiency of Perovskite Solar Cells Using a Nitrogen-Doped Graphene-Oxide-Treated Tin Oxide Layer. *ACS Appl. Mater. Interfaces* **2020**, *12*, 2417−23.
(195) Kakavelakis, G.; Maksudov, T.; Konios, D.; Paradisanos, I.; Kioseoglou, G.; Stratakis, E.; et al. Efficient and Highly Air Stable Planar Inverted Perovskite Solar Cells with Reduced Graphene Oxide Doped PCBM Electron Transporting Layer. *Adv. Energy Mater.* **2017**, *7*, 7.

https://doi.org/10.1021/acsomega.3c07994
ACS Omega 2024, 9, 12403−12425

(196) Yang, Z.; Xie, J.; Arivazhagan, V.; Xiao, K.; Qiang, Y.; Huang, K.; et al. Efficient and highly light stable planar perovskite solar cells with graphene quantum dots doped PCBM electron transport layer. *Nano Energy* **2017**, *40*, 345−51.
(197) Shin, D. H.; Kim, J. M.; Shin, S. H.; Choi, S.-H. Highly-flexible graphene transparent conductive electrode/perovskite solar cells with graphene quantum dots-doped PCBM electron transport layer. *Dyes Pigm.* **2019**, *170*, 107630.
(198) Li, H.; Tao, L.; Huang, F.; Sun, Q.; Zhao, X.; Han, J.; et al. Enhancing Efficiency of Perovskite Solar Cells via Surface Passivation with Graphene Oxide Interlayer. *ACS Appl. Mater. Interfaces* **2017**, *9*, 38967−76.
(199) Suragtkhuu, S.; Tserendavag, O.; Vandandoo, U.; Bati, A. S. R.; Bat-Erdene, M.; Shapter, J. G.; et al. Efficiency and stability enhancement of perovskite solar cells using reduced graphene oxide derived from earth-abundant natural graphite. *RSC Adv.* **2020**, *10*, 9133−9.
(200) Redondo-Obispo, C.; Ripolles, T. S.; Cortijo-Campos, S.; Álvarez, A. L.; Climent-Pascual, E.; de Andrés, A.; et al. Enhanced stability and efficiency in inverted perovskite solar cells through graphene doping of PEDOT:PSS hole transport layer. *Mater. Des* **2020**, *191*, 108587.
(201) Niu, J.; Yang, D.; Ren, X.; Yang, Z.; Liu, Y.; Zhu, X.; et al. Graphene-oxide doped PEDOT:PSS as a superior hole transport material for high-efficiency perovskite solar cell. *Org. Electron* **2017**, *48*, 165−71.
(202) Luo, H.; Lin, X.; Hou, X.; Pan, L.; Huang, S.; Chen, X. Efficient and Air-Stable Planar Perovskite Solar Cells Formed on Graphene-Oxide-Modified PEDOT:PSS Hole Transport Layer. *Nanomicro Lett.* **2017**, *9*, 39.
(203) Mann, D. S.; Seo, Y.-H.; Kwon, S.-N.; Na, S.-I. Efficient and stable planar perovskite solar cells with a PEDOT:PSS/SrGO hole interfacial layer. *J. Alloys Compd.* **2020**, *812*, 152091.
(204) Chowdhury, T. H.; Akhtaruzzaman, Md; Kayesh, MdE; Kaneko, R.; Noda, T.; Lee, J.-J.; et al. Low temperature processed inverted planar perovskite solar cells by r-GO/CuSCN hole-transport bilayer with improved stability. *Sol. Energy* **2018**, *171*, 652−657.
(205) Arora, N.; Dar, M. I.; Hinderhofer, A.; Pellet, N.; Schreiber, F.; Zakeeruddin, S. M.; et al. Perovskite solar cells with CuSCN hole extraction layers yield stabilized efficiencies greater than 20%. *Science (1979)* **2017**, *358*, 768−71.
(206) Lee, J.; Singh, S.; Kim, S.; Baik, S. Graphene interfacial diffusion barrier between CuSCN and Au layers for stable perovskite solar cells. *Carbon N Y* **2020**, *157*, 731−40.
(207) Sun, X.; Lin, T.; Song, Q.; Fu, Y.; Wang, Y.; Jin, F.; et al. Improved performance of hole-transporting layer-free perovskite solar cells by using graphene oxide sheets as the nucleation centers. *RSC Adv.* **2017**, *7*, 45320−6.
(208) Wang, Y.; Hu, Y.; Han, D.; Yuan, Q.; Cao, T.; Chen, N.; et al. Ammonia-treated graphene oxide and PEDOT:PSS as hole transport layer for high-performance perovskite solar cells with enhanced stability. *Org. Electron* **2019**, *70*, 63−70.
(209) Yeo, J.-S.; Kang, R.; Lee, S.; Jeon, Y.-J.; Myoung, N.; Lee, C.-L.; et al. Highly efficient and stable planar perovskite solar cells with reduced graphene oxide nanosheets as electrode interlayer. *Nano Energy* **2015**, *12*, 96−104.
(210) Jokar, E.; Huang, Z. Y.; Narra, S.; Wang, C.; Kattoor, V.; Chung, C.; et al. Anomalous Charge-Extraction Behavior for Graphene-Oxide (GO) and Reduced Graphene-Oxide (rGO) Films as Efficient p-Contact Layers for High-Performance Perovskite Solar Cells. *Adv. Energy Mater.* **2018**, *8*, 8.
(211) Yeo, J.-S.; Lee, C.-H.; Jang, D.; Lee, S.; Jo, S. M.; Joh, H.-I.; et al. Reduced graphene oxide-assisted crystallization of perovskite via solution-process for efficient and stable planar solar cells with module-scales. *Nano Energy* **2016**, *30*, 667−76.
(212) Kang, A. K.; Zandi, M. H.; Gorji, N. E. Fabrication and Degradation Analysis of Perovskite Solar Cells with Graphene Reduced Oxide as Hole Transporting Layer. *J. Electron. Mater.* **2020**, *49*, 2289−95.

https://doi.org/10.1021/acsomega.3c07994
ACS Omega 2024, 9, 12403−12425